Annals of Biomedical Engineering, Vol. 38, No. 2, February 2010 *(© 2010)* pp. 403–438
DOI: 10.1007/s10439-009-9814-y

Prediction of Extravascular Burden of Carbon Monoxide (CO) in the Human Heart

KINNERA ERUPAKA, EUGENE N. BRUCE, and MARGARET C. BRUCE

Center for Biomedical Engineering, University of Kentucky, Lexington, KY 40506-0070, USA

(Received 26 June 2008; accepted 26 September 2009; published online 16 October 2009)

Abstract—Clinically significant myocardial abnormalities (e.g., arrhythmias, S-T elevation) occur in patients with mild-to-severe carbon monoxide (CO) poisoning. We enhanced our previous whole body model [Bruce, E. N., M. C. Bruce, and K. Erupaka. Prediction of the rate of uptake of carbon monoxide from blood by extravascular tissues. *Respir. Physiol. Neurobiol.* 161(2):142–159, 2008] by adding a cardiac compartment (containing three vascular and two tissue subcompartments differing in capillary density) to predict myocardial carboxymyoglobin (MbCO) and oxygen tensions (P_cO_2) for several CO exposure regimens at rest and during exercise. Model predictions were validated with experimental data in normoxia, hypoxia, and hyperoxia. We simulated exposure at rest to 6462 ppm CO (10 min) and to 265 ppm CO (480 min), and during three levels of exercise at 20% HbCO. We compared responses of carboxyhemoglobin (HbCO), MbCO and P_cO_2 to estimate the potential for myocardial injury due to CO hypoxia. Simulation results predict that during CO exposures and subsequent therapies, cardiac tissue has higher MbCO levels and lower P_cO_2's than skeletal muscle. CO exposure during exercise further decreases P_cO_2 from resting levels. We conclude that in rest and moderate exercise, the myocardium is at greater risk for hypoxic injury than skeletal muscle during the course of CO exposure and washout. Because the model can predict CO uptake and distribution in human myocardium, it could be a tool to estimate the potential for hypoxic myocardial injury and facilitate therapeutic intervention.

Keywords—Myocardial oxygen tension, CO hypoxia, Exercise, Tissue oxygenation, Cardiac muscle, Skeletal muscle, Modeling.

INTRODUCTION

The major deleterious effect of carbon monoxide (CO) exposure is a decrease in oxygen (O_2) delivery to the tissues. CO-induced hypoxia can have profound effects on cerebral and myocardial oxygenation, resulting in neurological and cardiovascular injury. The neurological sequelae (headache, dizziness, confusion, nausea, loss of consciousness, and memory deficits) are well known.[15,85] Also, in recent years, myocardial injury, myocardial infarction, myocardial dysfunction and cardiac arrest have been reported in patients with mild to severe CO poisoning.[2,17,26,36,47,62,74,78,87] Myocardial injury in CO-poisoned victims,[26,47,74,87] was indicated by the presence of elevated cardiac injury biomarkers, e.g., troponin I, β-natriuretic peptide, creatinine kinase, and creatinine kinase-MB (myocardial band) and by ECG abnormalities, e.g., ST segment and T wave changes, sinus tachycardia, and premature atrial and ventricular contractions.[17,26,50,62] Observations of decreased left ventricular ejection fraction and right ventricular dysfunction after CO exposure imply myocardial dysfunction in these CO-poisoned patients.[26,47,74] The severity and duration of myocardial injury depend on the duration and amount of CO exposure.[66] Despite treatment after CO poisoning, cardiac sequelae often occur and these patients are thought to be at an increased risk of mortality due to myocardial injury.[36,62,87] There is also evidence that workers who are chronically exposed to CO have an increased risk for cardiovascular morbidity and mortality.[50,53,77]

In our previous modeling studies, Bruce and Bruce[9,10] compared the time courses of carboxymyoglobin (MbCO) and carboxyhemoglobin (HbCO) levels during and after CO exposures in a resting skeletal muscle compartment and in an "other tissue" compartment. These previous results[9,10] demonstrated that the equilibration of CO between vascular and extravascular tissues during CO exposure, as well as the removal of extravascular CO during therapy, occurred over a much longer time scale than did the major changes in the vascular CO content as represented by %HbCO. In our recent modeling study[8] we concluded that the slower rate of exchange of CO between blood and muscle tissues is due to the smaller blood–tissue conductance for CO and to the very small blood-to-tissue partial pressure gradients for CO. Thus, during exposures, MbCO increases more slowly than HbCO,

Address correspondence to Kinnera Erupaka, Center for Biomedical Engineering, University of Kentucky, Lexington, KY 40506-0070, USA. Electronic mail: kinnerarey@uky.edu

and during CO washout on room air, MbCO decreases more slowly than HbCO. These modeling studies also predicted that breathing 100% O_2 during washout causes a counterintuitive sudden rise in MbCO levels. Thus, the decrease in the CO content of myoglobin (Mb)-containing tissue may lag considerably behind the decrease in HbCO during therapy.

Cardiac muscle also contains Mb.[42] Because the heart is a rapidly contracting muscle with a high O_2 extraction fraction, it is very sensitive to O_2 deprivation.[41] High MbCO levels during CO washout on room air or 100% O_2 could contribute to significant hypoxia in the myocardium. Thus, analyzing the temporal changes in HbCO, MbCO, and P_cO_2 levels in the vascular and extravascular compartments of the heart will aid in estimating the potential for hypoxic myocardial injury and facilitate therapeutic intervention. The main objective of this study was to develop a validated model for predicting time varying O_2 tensions and CO levels in human myocardium and skeletal muscle tissue during exposure to low (265 ppm) and high (6462 ppm) CO concentrations for exposures lasting from a few minutes to a few hours, during which subjects were either at rest or exercising.

The model developed in this study is an enhancement of our previous models. Our earliest model[9] consisted of five lumped compartments: arterial blood (ar), lungs (L), skeletal muscle (m), nonmuscle tissue (ot), and mixed venous blood (mx). Recently this early model was upgraded[8] by subdividing the single lumped muscle compartment into two communicating subcompartments (m_1, m_2) so that intra-tissue diffusion of gases (O_2 and CO) and arterio-venous shunting could be taken into account. The new model described herein (see Methods, Fig. 1a) adds a cardiac muscle compartment to the upgraded model.

Because the severity of myocardial injury during CO-induced hypoxia is dependent on the duration and concentration of the CO exposure, the new model was used to predict O_2 tensions and MbCO levels in the myocardium for various simulated CO exposure conditions. Also, exercise increases ventilation which, in turn, increases the amount of CO inhaled. Therefore, exercise during CO exposure could further increase the risk for hypoxic injury. Thus, CO exposure (20% HbCO) during moderate exercise was simulated to explore the mechanistic basis for the increased risk of cardiac injury in this situation. When considering the possible treatment strategies for CO-poisoning victims, it is not always clear whether hyperbaric oxygen therapy is necessary because the treatment strategy is determined primarily by the HbCO levels on admission to the hospital. The %HbCO, a key factor in determining the treatment protocol, is a limited measure of poisoning severity although it can be readily determined. Myocardial O_2 tension and myocardial CO load (%MbCO), which are more direct indicators of myocardial O_2 availability, are difficult to measure noninvasively.[8] Therefore, to explore the effects of specific treatment strategies on the myocardium our simulation studies also assessed the degree of myocardial hypoxia resulting during normoxic and hyperoxic therapies.

METHODS

Description of the Whole Body Model of O_2 and CO Exchange

The model used in the current study is an expansion of our previous model.[8] A significant enhancement to that model is the addition of the cardiac compartment (Fig. 1a). All symbols, variables, and parameters are summarized in Appendix A. CO and O_2 mass balance equations were written for all compartments (Eqs. B.1–B.28, Appendix B). CO and O_2 entering through the lungs are transported via the major arteries of the arterial blood compartment to the vascular compartments of skeletal muscle (bm_1, bm_2, bm_3), cardiac muscle (bc_1, bc_2, bc_3), and non-muscle tissue (bot). CO and O_2 then diffuse into the tissue compartments (m_1, m_2, c_1, c_2, ot), driven by pressure gradients. Determining the partial pressures of O_2 and CO, and O_2 flux in each blood compartment of the model is done by solving the oxyhemoglobin dissociation curve, Haldane's equation, and blood-to-tissue O_2 flux equations, at each time step using an iterative approach (see section "Special Functions", Appendix B).[8] The Haldane equation describes the competition of CO and O_2 for hemoglobin (Hb) and Mb binding sites.[9] Determination of the circulatory transport time delays for the arterial and mixed venous compartment, and mixing of blood in the vascular compartments, has been explained in detail in our initial model[9] (see auxiliary equations in Appendix B).

Cardiac Compartment Structure and Parameter Estimation

Like skeletal muscle,[8] the cardiac compartment of the model comprises three vascular subcompartments (bc_1, bc_2, bc_3) and two cardiac tissue subcompartments (c_1, c_2) (Fig. 1b). The concept of the two compartment model was introduced to allow diffusion of O_2 within the tissue and to implement indirect arterio-venous shunting. The tissue subcompartment, c_1 (20% of cardiac tissue volume, V_c), is envisioned as tissue perfused extensively by small arterioles and venules in vascular subcompartments bc_1 and bc_3 as well as by

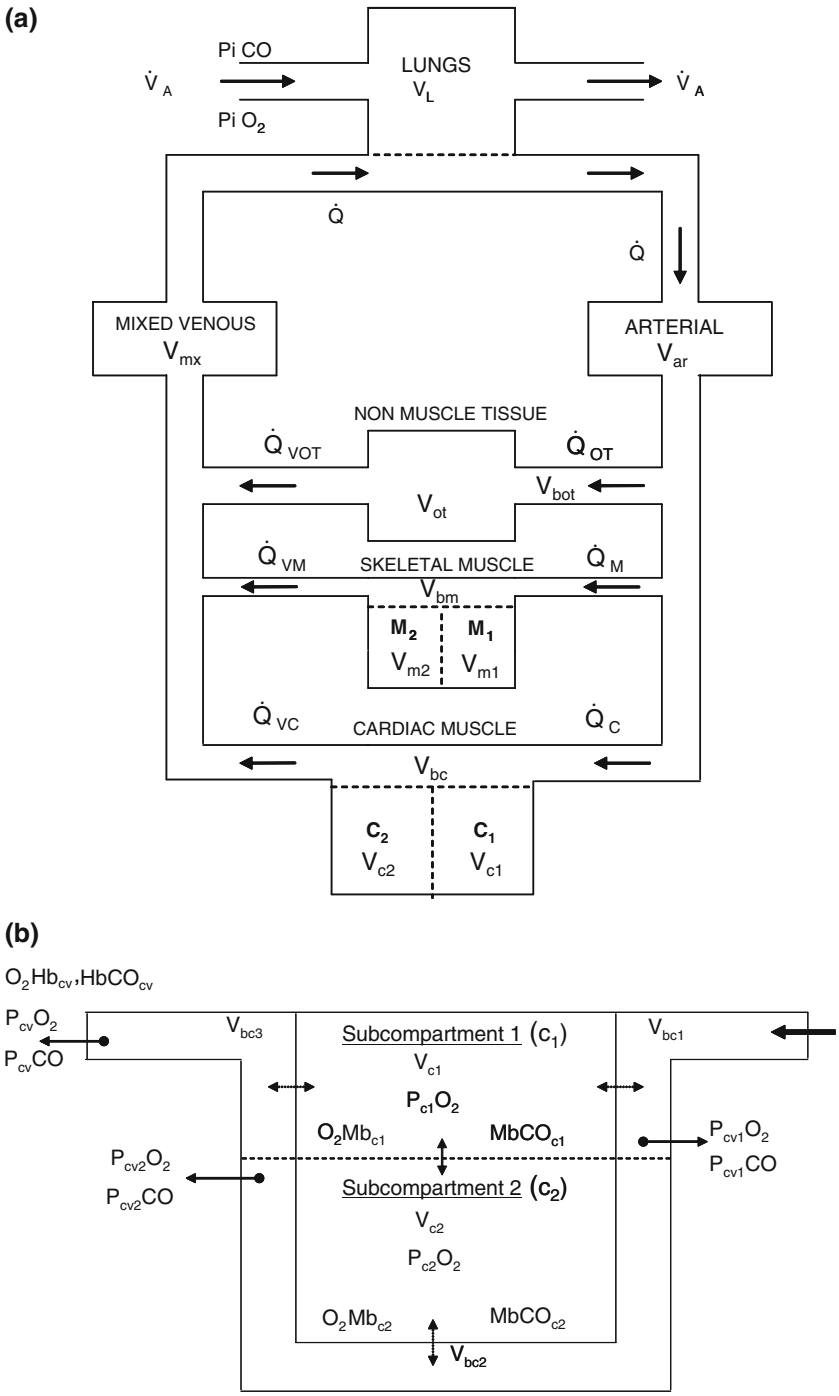

FIGURE 1. (a) Model architecture. Overall structure of the model, which expands our previous model[8] by adding a cardiac compartment. The new model consists of six major compartments: lungs, arterial blood, mixed venous blood, non-muscle tissue, skeletal muscle tissue with two subcompartments, and cardiac tissue with two subcompartments. For details of the cardiac compartment see Fig. 1b, and for the symbols see Table A1, Appendix A. (b) Structure of Cardiac compartment. The cardiac compartment is divided into two extravascular subcompartments (c_1, c_2) and three vascular subcompartments (bc_1, bc_2, bc_3). Arterial blood enters the vascular subcompartment bc_1 as $\dot{Q}_c$. Dotted double arrows indicate blood–tissue gaseous fluxes driven by partial pressure gradients. Solid double arrows indicate diffusive gaseous fluxes driven by concentration gradients of dissolved gases. For details about the calculation of fluxes see text and Appendix B. For symbols see Tables (A1)–(A2) of Appendix A.

capillaries. The tissue subcompartment, c_2 (80% of cardiac tissue volume, V_c), is assumed to be perfused mostly by capillaries in vascular subcompartment bc_2. The volumes of the tissue subcompartments, V_{c1} and V_{c2}, and the volumes of the vascular subcompartments, V_{bc1}, V_{bc2}, and V_{bc3}, were chosen after various

TABLE 1. Experimental data for myocardial oxygen tensions.

Source	Species	P_aO_2 (Torr)	$P_{cv}O_2$ (Torr)	P_cO_2 (Torr)	MBF (mL 100 g^{-1} min^{-1})	MOC (mL 100 g^{-1} min^{-1})
[20]	Human	99	17.3	–	118	15
[20]	Human	42	15.7	–	167	17
[23]	Swine	359	–	112 ± 8.5	94	6.7
[27]	Dog	326	–	49/26	0.8	0.1
[27]	Rat	99	–	40/20	4.5	0.54
[27]	Rat	89	–	15/35	4.5	0.54
[29]	Swine	99	–	49 ± 2	94	6.7
[31]	Rat	87	20	25	233.1	39.6
[33]	Swine	103	27.33	50/31	94	6.7
[33]	Swine	57	22.77	35	129.7	5.69
[33]	Swine	44	19.75	26	147.6	5.96
[38]	Swine	90	23.25	46 ± 7.5	94	6.7
[39]	Dog	143	46	42 ± 7	0.8	0.1
[40]	Swine	150	–	30.3 ± 4.7	94	6.7
[58]	Dog	93.5	18.8	43/17	90	6.6
[58]	Dog	63.7	18.3	40/15	–	–
[60]	Swine	150	–	42 ± 5.6	94	6.7
[81]	Rat	99	–	10	4.5	0.54
[82]	Rat	99	–	48/18	4	0.4
[84]	Swine	189	31.8	–	125	11.3
[84]	Swine	39	21	–	175	12.5
[84]	Swine	40	17	–	173	9.8
[92]	Dog	32	22	–	160	9.79
[92]	Dog	27	18	–	210	6.7

P_cO_2 = Myocardial tissue PO_2.

volume distributions were tested to optimize the model predictions for myocardial blood and tissue O_2 tensions (Table 1). Model predictions for myocardial tissue and blood O_2 tensions were estimated for simulation conditions presented in Table 1 for multiple values of relative volume, F_{vc}. The tested range of relative volume ($F_{vc} = V_{c1}/[V_{c1} + V_{c2}]$) was 0.1–0.9. The value of $F_{vc} = 0.2$ was chosen based on visual fit to the data of Table 1. The volume of the second myocardial blood compartment, V_{bc2}, is 80% of the total myocardial volume, V_{bc}. The remaining 20% of the myocardial blood volume is distributed between the first, bc_1, and third, bc_3, vascular subcompartments. To account for arterial-venous diffusive shunting through tissue compartment c_1, we assumed that V_{bc3} is 9.5% (D_{bvc_on}) of V_{bc1}. The experimentally measured coronary blood volume in the arterial compartment and the combined blood volumes in coronary capillary and venous compartments reported by Kassab *et al.*[48] agree with the model blood volume in V_{bc1} and V_{bc2}, respectively, when F_{vc} is 0.2.

The total myocardial metabolic rate, MR_cO_2, is distributed between the two subcompartments in proportion to their tissue volumes. The arterial blood, with a partial pressure of O_2, PaO_2, flows into the first vascular subcompartment, bc_1. O_2 in blood continuously diffuses into the cardiac subcompartment c_1 because O_2 is being utilized by the tissue to meet its O_2 metabolic demand, $MR_{c1}O_2$. It is assumed that O_2 diffuses from bc_1 to c_1 at a rate of O_2flux_{c1}, which is the product of the O_2 diffusion coefficient, $Db_{c1}O_2$, and O_2 pressure difference (Eq. B.19, Appendix B). This phenomenon establishes O_2 concentrations of $C_{c1}O_2$ and $C_{cv1}O_2$ in c_1 and bc_1 subcompartments, respectively. In all tissue compartments containing Mb, O_2 bound to Mb is considered in addition to the dissolved O_2 concentrations.[8] O_2 diffuses from vascular compartment bc_2 to tissue subcompartment c_2 at a rate of O_2flux_{c2} with a diffusion coefficient of $Db_{c2}O_2$. The metabolic demand for O_2, $MR_{c2}O_2$, of this tissue compartment is met by diffusion of O_2 from blood compartment bc_2 and also by intra-tissue diffusion from the tissue compartment, c_1, where the intra-tissue diffusion coefficient is D'_cO_2. Diffusion of O_2 establishes concentrations $C_{c2}O_2$ and $C_{cv2}O_2$ in the second tissue and blood subcompartments, respectively. Based on the pressure gradients established between c_1 and bc_3, O_2 diffuses between these compartments at a rate of O_2flux_{c3}, with a coefficient of $Db_{c3}O_2$, ($D_{bvc\_on} \cdot Db_{c1}O_2$) resulting in concentration $C_{cv3}O_2$ in bc_3. Because O_2 diffusivity is similar in plasma and muscle tissue,[61] the model assumes that O_2 diffusion coefficients from blood to tissue, or vice versa, are equal. (For details see Eqs. B.15–B.24 and auxiliary equations in section "Cardiac Muscle Compartment" of Appendix B; Tables A1–A4 in Appendix A.)

The effective blood to tissue conductance for O_2 depends on the permeability-surface area product (PS) of the tissue subcompartments c_1 and c_2 ($PS_{c1}O_2$, $PS_{c2}O_2$), respectively. The PS for O_2 for cardiac muscle was estimated as 200 mL min^{-1} $Torr^{-1}$ g^{-1} by Li *et al.*[57] For our model, best estimates for myocardial tissue PO_2 predictions were obtained when $PS_{c1}O_2$ and $PS_{c2}O_2$ were 180 and 450 mL min^{-1} $Torr^{-1}$ g^{-1}, respectively. Cladwell *et al.*[12] have reported an increase in PS with increases in blood flow. Thus, in our model, PS increases with increases in blood flow to the tissue (see auxiliary equations in section "Cardiac Muscle Compartment" of Appendix B). The mean diffusion distance in skeletal muscle in our previous model is 0.1 cm.[8] The capillary density in cardiac muscle is approximately 8 times that of skeletal muscle,[32] thus the mean diffusion distance for the cardiac compartment was estimated as 0.0353 cm ($0.1/\sqrt{8}$).

Values for most of the parameters for our expanded model were those used in and referenced in our previous publications.[8,9] A regression equation for estimation of blood volume was also included in the model.[56] In addition, predictive equations for estimation of cardiac output[3,4,6,18,21,34,37,72] ($\dot{Q}$) and heart rate[14,50,83] (HR) as a function of total body oxygen consumption (MRO_2) were also developed (Eqs. C.4 and C.6, Appendix C) but were used only when values were not provided by the investigators whose data we simulated. The design of the cardiac compartment is parallel to that of the skeletal muscle compartment[8] but differs in the values of physiological parameters. Regression equations were developed for the estimation of myocardial oxygen consumption[30,43,44,49,65,67] (MOC) and myocardial blood flow[54] (MBF) from heart rate (Figs. 2 and 3). Parameter estimation, development of predictive equations (MOC, MBF), and validation of tissue O_2 tensions were done for the left ventricular region (left ventricle and intraventricular septum) of the heart. Data used for developing the regression equations to estimate MOC, MBF, $\dot{Q}$, and HR were obtained from experiments conducted at zero CO exposure levels.

In estimating the parameters for the cardiac compartment we assumed that in healthy adults under normal, ambient conditions, the average myocardial PO_2 does not fall below 22 Torr[22,64,84] at rest and does not fall below 6 Torr during maximal exercise. Richardson *et al.*,[69,70] reported a PO_2 of 3–5 Torr in maximally exercising skeletal muscle, so we anticipated that PO_2 would be at least 6 Torr in the cardiac muscle (as cardiac muscle has a higher capillary density, blood flow and O_2 consumption than skeletal muscle). Choosing F_{vc} as 0.2 and PS as 180 mL min^{-1} $Torr^{-1}$ g^{-1} ($PS_{c1}O_2$) and 450 mL min^{-1} $Torr^{-1}$ g^{-1} ($PS_{c2}O_2$) for the cardiac compartment guaranteed that the model-estimated O_2 tension fulfilled the assumptions stated above for a range of healthy, normal subjects.

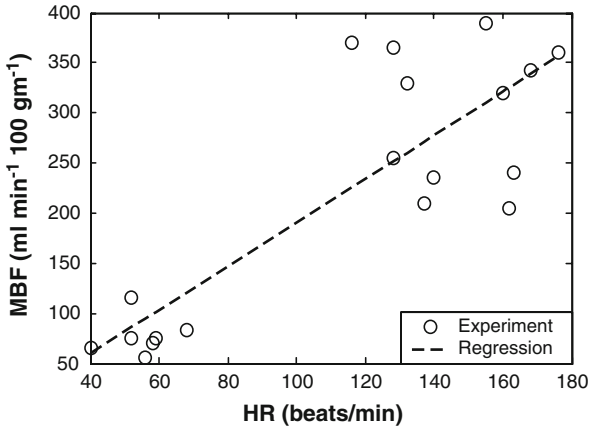

FIGURE 2. Myocardial blood flow (MBF) vs. heart rate (*HR*). Experimental data (o) are from Laaksonen *et al.*[54] The regression line is given by MBF = 2.18(*HR*) − 27.3.

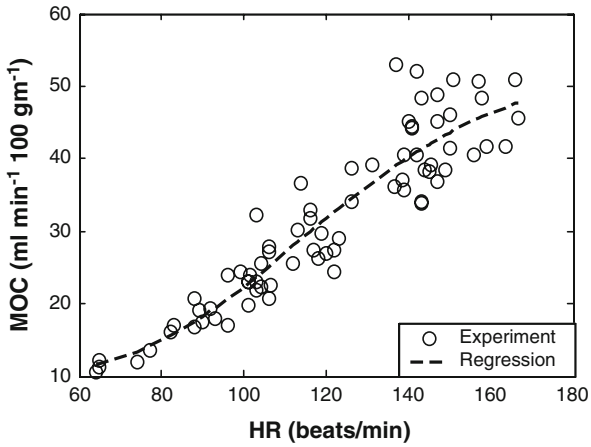

FIGURE 3. Myocardial oxygen consumption (MOC) vs. heart rate (*HR*). Symbols: MOC's (corrected using the procedure described in text). The regression equation (dashed line) is given by $MOC = \frac{46.6}{1 + \left(\frac{122.7}{HR}\right)^{4.85}} + 9.76$.

Predictive Equations

Prediction formulas were developed to estimate MOC[30,43,44,49,65,67] and MBF[54] as functions of HR based on rest and exercise data obtained from the literature. These experiments used the nitrous oxide (N_2O) method to measure MBF. However, the N_2O method was reported to under-estimate true blood flow.[73] Implementation of the prediction equation for MBF based on the N_2O method resulted in a mismatch of supply and demand for O_2 in the myocardium and predicted tissue PO_2 values that were too low. Thus, to predict the MBF, data from Laaksonen *et al.*[54] were used. In their study, dynamic PET (Positron Emission

Tomography) accompanied by intravenous injection of labeled water ([^{15}O] H_2O) was used to measure MBF. To develop the predictive formulas for MBF and MOC, we constructed a regression relation for MBF as a function of *HR* with data from reference 54, as shown in Fig. 2. We then calculated corrected MOC from studies using the N_2O method by first recalculating the arterio-venous (a-v) difference of O_2 content as the ratio of measured MOC and measured MBF,[30,43,44,49,65,67,73] and then recalculating MBF from the heart rates (Goodale and Hackel,[30] Jorgensen *et al.*,[43] Jorgensen *et al.*,[44] Kitamura *et al.*,[49] Nelson *et al.*,[65] Regan *et al.*,[67] Sapirstein and Ogden[73]) using the developed predictive formula for estimating MBF described above (Fig. 2). Finally, MOC was calculated as the product of a-v difference and recalculated blood flow. A non-linear curve fit was done on the corrected data using MATLAB 6.5 to establish MOC as a function of heart rate as shown in Fig. 3.

Sensitivity Analysis

The current model has 28 nonlinear differential equations and 123 parameters. Nominal values for most of the parameters were obtained from the literature (Table A4, Appendix A) or directly from the investigators[7,11,50] whose data we simulated, e.g., MRO_2, *HR*, $\dot{Q}$ (Table A3, Appendix A). In some cases, parameters were estimated with average values from a group of subjects or published predictive formulas, e.g., volume of heart muscle, myocardial blood volume, myocardial Mb concentration (Table A4, Appendix A). Some parameter values were also estimated from predictive formulas described above, e.g., MOC, MBF (Eqs. C.1–C.8, Appendix C). Some parameters, such as *PS*, change their values during a simulation run (see auxiliary equations in sections "Skeletal Muscle Compartment" and "Cardiac Muscle Compartment", Appendix B). Other parameters, e.g., F_{vc} and D_{bvc_on}, represent quantities that are very difficult or impossible to measure (Table A4, Appendix A).

Sensitivity analysis helps to determine the level of accuracy needed for a parameter to make the model valid and estimates the effects of parameter variations on model predictions. The process involves observing the relative changes in the model response by varying one model parameter over a reasonable range while keeping all other parameters constant. Thus, sensitivity analysis was performed to analyze the effects of MOC, MBF, *PS*, F_{vc}, D_{bvc_on}, d_{xc}, and D_MCO on the model predictions of myocardial tissue PO_2 ($P_{c_1}O_2$, $P_{c_2}O_2$) and coronary venous PO_2 ($P_{cv}O_2$).

In order to observe changes in the model response for variations of a single parameter, a baseline steady-state was simulated for a healthy, sedentary human subject (subject 19 of Kizakevich *et al.*[50], age: 22 years; height: 1.8 m; weight: 69.5 kg; $\dot{Q}$: 6.68 L/min; MRO_2: 170 mL/min; *HR*: 77 beats/min; 2% HbCO; all other parameters are from Table A4, Appendix A. The model predictions for myocardial and skeletal ($P_{m_1}O_2$, $P_{m_2}O_2$) tissue O_2 tensions at the baseline steady-state are 31, 18, 40.5, and 27 Torr in c_1, c_2, m_1, and m_2, respectively. The baseline steady-state $P_{cv}O_2$ and skeletal muscle venous ($P_{mv}O_2$) PO_2's are 20 and 29 Torr, respectively. When a sensitivity analysis was performed it was found that the myocardial tissue and vascular O_2 tensions are most sensitive to MOC, MBF, F_{vc}, and *PS*. The tissue O_2 tensions varied in direct proportion with changes in MBF and *PS* and in inverse proportion with MOC and F_{vc}. Model predictions for coronary venous PO_2's were most sensitive to changes in MOC and MBF. The effects of D_{bvc_on} and d_{xc} on the vascular and tissue O_2 tensions are negligible. The sensitivity of model predictions to D_MCO has been discussed in our previous models.[8–10]

An increase in *PS* by 50% of its baseline steady-state value (Table A4, Appendix A) resulted in an increase in steady-state O_2 tensions of the c_1 and c_2 subcompartments by 15.6 and 11.7%, respectively. A decrease in the *PS* by 50% of its baseline steady-state value resulted in a decrease of the steady-state O_2 tensions by 46.8% in c_1 and 39.7% in c_2. Model predictions of myocardial O_2 tensions in the subcompartments are sensitive to $PS_{c_1}O_2$ in the range of 100–500 mL min^{-1} Torr^{-1} g^{-1} and to $PS_{c_2}O_2$ in the range of 300–1300 mL min^{-1} Torr^{-1} g^{-1} (Figs. 4a, 4b). A change in F_{vc} from 0.2 to 0.1 resulted in an increase in cardiac tissue PO_2's by 27% (c_1) and 8.3% (c_2) from their baseline steady-state values.

An increase in F_{vc} from 0.2 to 0.3 decreased the steady-state myocardial tissue O_2 tensions by 16.8 and 7% in c_1 and c_2 subcompartments, respectively. Thus, an increase in F_{vc} causes the O_2 tensions in the myocardial subcompartments to decrease. Also, changes in F_{vc} have a greater effect on the model predictions of O_2 tensions of the first subcompartment than those of the second subcompartment (Figs. 4a, 4b).

Estimation of MBF is sensitive to the slope (m) of the regression equation $\text{MBF} = mHR - C$ (see Fig. 2). Figure 4c shows that increasing the slope, m, of the regression relation to estimate MBF as a function of *HR* increases the tissue and vascular O_2 tensions. Also, there may be variability in the estimated MBF at higher levels of *HR* (Fig. 2), which may influence the predicted O_2 tensions in the heart. At a *HR* of 116 beats/min, a variation of ±5% in the MBF estimated using the regression equation will result in an increase (+5% variation in MBF) in $P_{c_1}O_2$, $P_{c_2}O_2$, and $P_{cv}O_2$ to 17.9, 10.9, and 13.5 Torr, respectively, and a decrease

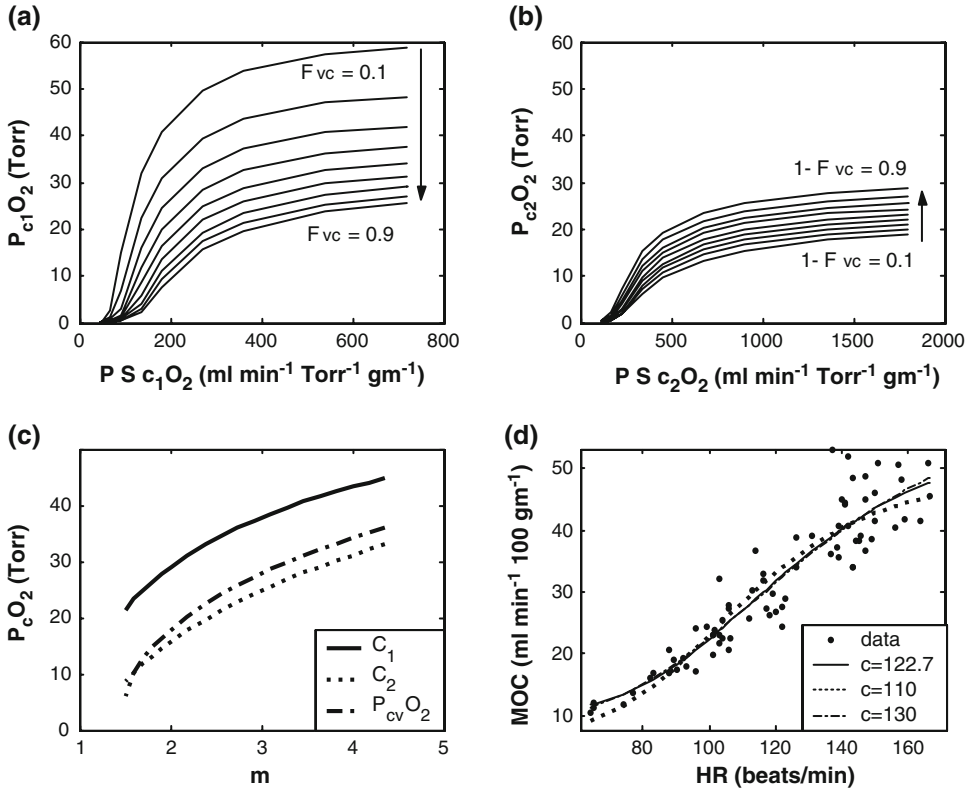

FIGURE 4. Sensitivity analysis. (a) $P_{c1}O_2$ vs. $PS_{c1}O_2$ for a range of F_{vc} (0.1–0.9, top to bottom). (b) $P_{c2}O_2$ vs. $PS_{c2}O_2$ for a range of F_{vc} (0.1–0.9, top to bottom). (c) Model predictions of O_2 tensions (Ordinate), $P_{c1}O_2$, $P_{c2}O_2$, $P_{cv}O_2$ are sensitive to slope, *m*, (abscissa) of the regression relation used to estimate MBF from *HR* (refer to Fig. 2). (d) Curve fit to the experimental data (points) of MOC vs. *HR* for different values of the parameter *c*.

TABLE 2. Effect of variation in MBF on myocardial tissue and venous O_2 tensions.

ΔMBF%	$P_{c1}O_2$ (Torr)	$P_{c2}O_2$ (Torr)	$P_{cv}O_2$ (Torr)
−20	4.7	2.8	5.96
−10	10.3	5.99	10.3
0	15.6	9.33	13.5
10	20.1	12.4	15.9
20	24.1	15.1	17.9
35	29.0	18.5	20.6

ΔMBF = Variation in MBF.

(−5% variation in MBF) in $P_{c1}O_2$, $P_{c2}O_2$, and $P_{cv}O_2$ to 13, 7.7, and 12 Torr, respectively (see Table 2).

The prediction equation for estimating MOC as function of *HR* is of the form $MOC = ([a - d]/[1 + \{c/HR\}^b]) + d$. Estimation of MOC is sensitive to changes in parameter '*c*' of the equation above for a range of resting *HR* (60–85 beats/min). A best curve fit to the experimental data of Fig. 3, with a least mean square error criterion, was obtained at $c = 122.7$ ($a = 56.3$, $b = 4.85$, $d = 9.76$). Fixing the value of *c* at 110 and fitting a curve ($a = 49.9$, $b = 5.2$, $d = 6.7$) to the experimental data of Fig. 3 resulted in a decrease of MOC by 11% of its baseline steady-state value at a *HR* of 77 beats/min (Fig. 4d). An 11% decrease in MOC increased myocardial coronary venous and tissue PO_2's by 12% (cv), 16.7% (c_1), and 12.2% (c_2), respectively.

Simulation Software

ACSL™ version 11.8 was used for implementing the model. A Runge–Kutta–Fehlberg variable step size algorithm with error flagging was used for numerical integration. Convergence of the algorithm was tested for various step sizes and the maximum allowable step size was determined to be 0.001 min. Simulations were performed in double precision and a 12 min stabilization period was initiated with every simulation run for the baseline simulation to reach a steady state.

RESULTS

Validation of the Cardiac Compartment

We compiled experimental studies which provided values for myocardial tissue and coronary venous PO_2's. Most of the data were obtained from studies on anesthetized animals, but myocardial PO_2 values were also available from studies involving human

subjects.[20,22,64] The myocardial O_2 tensions in the literature were usually reported as histograms or as mean values with standard deviations. We considered the mean PO_2 of the upper half of a histogram (above the mean value) or the reported mean PO_2 plus one standard deviation as the O_2 tension of myocardial subcompartment c_1. The mean PO_2 corresponding to the lower half of the histogram (below the mean value) or the reported mean PO_2 minus one standard deviation was considered to be the O_2 tension of myocardial subcompartment c_2. When average O_2 tensions were the only values reported, PO_2's < 22 Torr in normoxia were considered to be measured in c_2. Also, the site of measurement of PO_2 was taken into consideration, i.e., when the measuring electrode was close to an arteriole or capillary, the PO_2 was assumed to represent c_1 or c_2, respectively. The PO_2 of the third vascular subcompartment of the cardiac compartment, bc_3, (i.e., the blood leaving the heart compartment), was compared to coronary venous PO_2 reported in the experimental data.

Predicted PO_2's from the model were tested for conditions of normoxia, hyperoxia and mild to severe hypoxia. In order to compare the model predictions with the experimental data, studies from Table 1 were simulated with the enhanced model. Inspired levels of O_2 in the simulations were set equal to the reported experimental values and ventilation was adjusted to achieve the reported experimental arterial PO_2 (P_aO_2) in the steady state. Arterial PO_2's for hypoxia ranged from 27 to 89 Torr. Normoxic arterial PO_2's were considered in the range of 90–103 Torr. Arterial PO_2's for hyperoxia ranged from 121 to 468 Torr. For all simulations the volume distribution fraction, F_{vc}, was 0.2 and *PS* values for the first and second cardiac tissue compartments were 180 and 450 mL min^{-1} Torr^{-1} g^{-1}, respectively. Measured values for MBF and MOC were reported in the studies cited (Table 1).

Figure 5 shows the comparison of model predictions (myocardial tissue and coronary venous PO_2's) with experimentally measured values. In Fig. 5a, the model-predicted PO_2's for myocardial tissue subcompartment 1 ($P_{c1}O_2$) are slight overestimates of the experimental data. The model predictions for subcompartment 2 ($P_{c2}O_2$) myocardial tissue O_2 tensions on average are slight underestimates of experimental data as seen in Fig. 5b. Overall, considering the limited availability and variability of experimental data (Table 1) for myocardial O_2 tensions, the model closely represents the trends in the data. As seen in Fig. 5c, the model predictions of coronary venous O_2 tensions ($P_{cv}O_2$) fit variations in the experimental coronary venous PO_2 for a wide range of arterial PO_2 (27–468 Torr). Thus, the model predicts physiologically reasonable myocardial tissue and vascular O_2 tensions over a wide range of arterial PO_2 values.

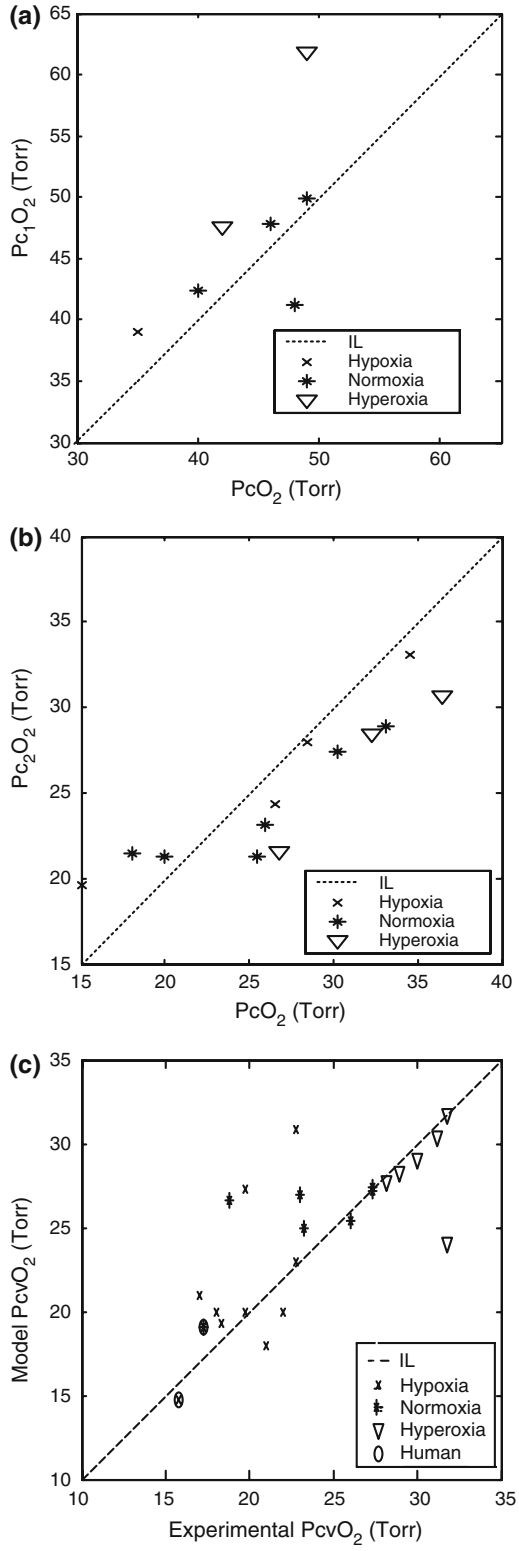

FIGURE 5. Validation of myocardial tissue and blood O_2 tensions. Abscissa: Experimental O_2 tensions (Table 1). Ordinate: Model predicted O_2 tensions. The dashed lines are identity lines (IL). (a) Myocardial PO_2 of tissue subcompartment 1, $P_{c1}O_2$. (b) Myocardial PO_2 of tissue subcompartment 2, $P_{c2}O_2$. (c) Myocardial coronary venous PO_2, $P_{cv}O_2$.

Re-evaluation of Our Previous Simulation Results

Our previous simulations of CO exposure studies were repeated to ensure that the new model fits these experimental data similarly to our earlier, simpler models. After validating the cardiac compartment, the ability of the enhanced model to reproduce experimental data from (i) transient CO exposure followed by washout and (ii) hyperoxic rebreathing was tested as these two situations represent the extremes of time resolution which the model needs to achieve. Re-evaluation of our previous simulations using the new model also made possible the estimation of O_2 and CO levels in the myocardial tissue and vascular subcompartments during transient CO exposure, washout, and hyperoxic rebreathing situations.

Simulation of Transient CO Exposure

Benignus *et al.*[7] exposed human subjects to a high concentration of CO (6683 ppm) in room air for 4–6 min, followed by washout on air for 4–5 h. Many subject-specific parameters were provided by the investigators (Table A3, Appendix A). Total body O_2 consumption (233 mL/min) and the diffusion coefficient for CO were from our previous model.[8] MBF and MOC were estimated from the prediction equations developed (see Methods or Eqs. C.7–C.8 of Appendix C).

The enhanced model fits the experimental HbCO data similarly to our earlier models, as shown in Fig. 6a, and predictions of skeletal muscle tissue O_2 tensions and MbCO levels of the enhanced model were in agreement with the predictions of the earlier model. Model predicted MbCO levels in the subcompartments of skeletal (%$MbCOm_1$, %$MbCOm_2$) and myocardial tissue (%$MbCOc_1$, %$MbCOc_2$) are shown in Figs. 6b and 6c. As shown in Fig. 6, the MbCO levels in both subcompartments peak earlier in cardiac muscle than in skeletal muscle. High levels of MbCO are observed for greater lengths of time in the skeletal muscle in comparison to the cardiac muscle compartment. In skeletal muscle, the MbCO levels of subcompartment 2 are initially lower than subcompartment 1, but gradually increase and approximate the MbCO levels of subcompartment 1. The content of CO is higher in cardiac subcompartment 2 than in subcompartment 1 during CO uptake and washout on room air. For air

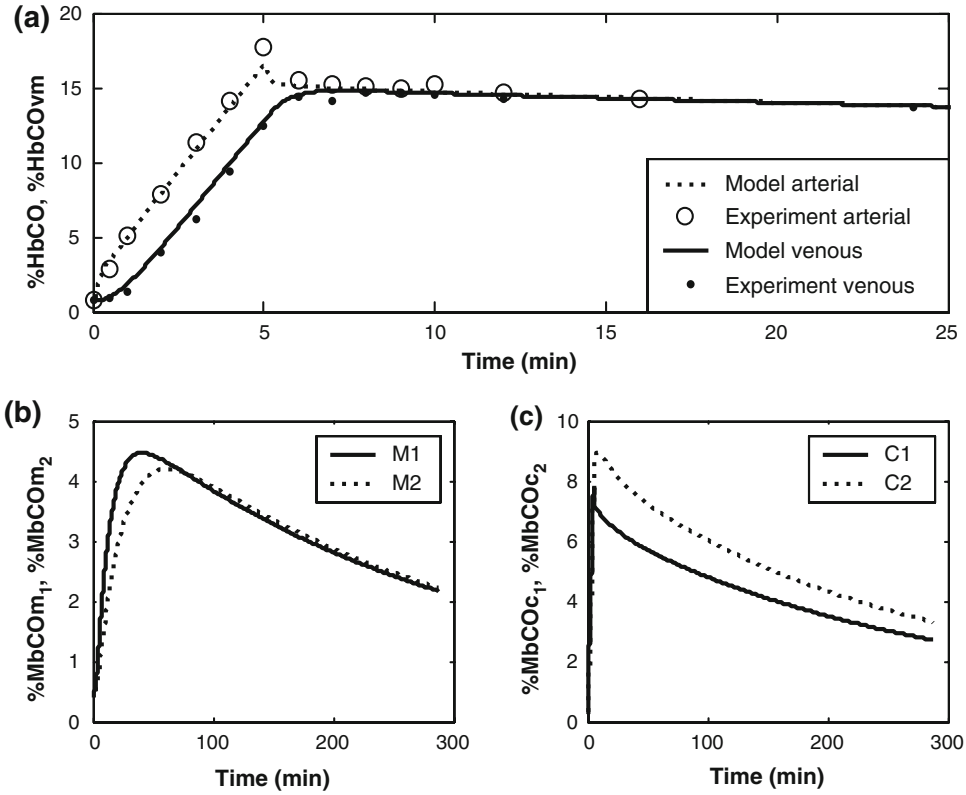

FIGURE 6. Simulation of 5-min CO exposure (6683 ppm) and washout for 480 min on room air. (a) Arterial (○) and muscle venous (•) %HbCO vs. time (subject 120 from Benignus *et al.*[7]), and model predictions (*lines*). (b) Skeletal muscle MbCO levels of tissue subcompartment 1, m_1 (*solid line*) and subcompartment 2, m_2 (*dashed line*). (c) Cardiac muscle MbCO levels of tissue subcompartment 1, c_1 (*solid line*) and subcompartment 2, c_2 (*dashed line*). Results are shown on 2 time scales to compare both rapid (% HbCO in a) and slow behaviors (%MbCO in b–c). Parameter values for this simulation are given in Table A3 of Appendix A.

(and hyperoxic) washout, the peak MbCO levels in the skeletal and cardiac compartments occur during the washout phase.

When compared to the pre-CO exposure state, in skeletal muscle the O_2 tension drops by 16.5% in the first subcompartment (m_1) and by 23.9% in the second subcompartment (m_2) at the end of CO exposure. In contrast, the myocardial O_2 tensions in the first and second subcompartments decrease more, by 21.3 and 37.5%, respectively, at the end of CO exposure when compared to the pre-CO exposure state. After CO exposure followed by 4 h of room air washout, all the PO_2's are still 2–3 Torr below their pre-exposure levels. The tissue O_2 tensions are slightly lower at the time of peak MbCO levels, which occur during the CO washout phase when HbCO is below its peak rather than at the end of the CO exposure. The O_2 tensions of skeletal and myocardial tissue are better correlated with peak MbCO levels than with the decreasing HbCO levels.

Simulation of CO Rebreathing in Hyperoxia

Burge and Skinner[11] conducted CO rebreathing experiments in hyperoxia to estimate total blood volume. Subjects in this study rebreathed 60–70 mL of CO in ≥99% O_2 for 40 min. Subject-specific parameter values for their subject 2[8–10] were provided by the investigators (Table A3, Appendix A).[11] Estimates for other unknown parameters were obtained from predictive equations in this study (Appendix C) and also from our previous models.[8–10] Figure 7a shows that the model fits data similarly to the simulation results of our previous models. As shown in Fig. 7, the MbCO levels in the cardiac subcompartments peak earlier than in the skeletal muscle after which they begin to decrease gradually. CO content is higher in the first than in the second subcompartments of the skeletal and myocardial tissues due to the higher MbCO levels. The skeletal and myocardial tissue O_2 tensions are high due to breathing of ≥99% O_2.

Effects of Concentration of CO and Duration of Exposure

Long-term sequelae of myocardial injury have been reported to be dependent on the duration and amount of CO exposure.[66] Despite treatment after CO poisoning, neurological and cardiac sequelae often occur. The enhanced model was used to simulate two different kinds of CO exposures that resulted in similar peak

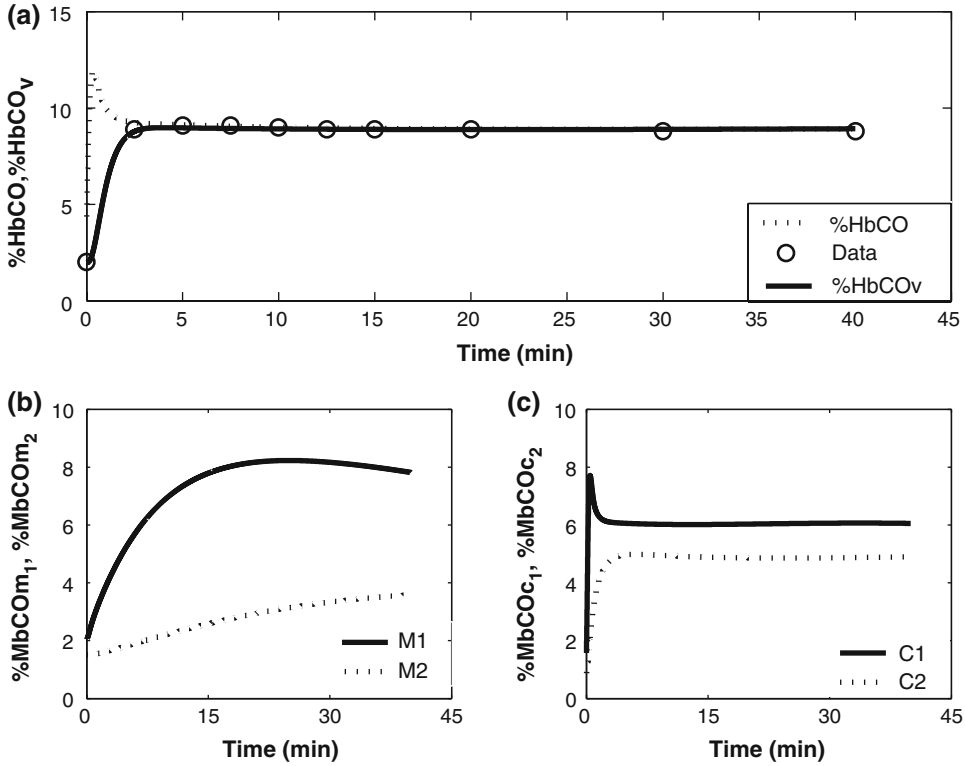

FIGURE 7. Simulation of CO rebreathing in hyperoxia. (a) Muscle venous %HbCO vs. time during CO rebreathing. Model prediction (*solid line*) and measured values from antecubital vein (○), subject #2 from Burge and Skinner.[11] Also the model prediction for arterial %HbCO (*dashed line*) is shown. (b) Predicted skeletal muscle MbCO levels of tissue subcompartment 1, m_1 (*solid line*) and subcompartment 2, m_2 (*dashed line*). (c) Predicted cardiac muscle MbCO levels of tissue subcompartment 1, c_1 (*solid line*) and subcompartment 2, c_2 (*dashed line*). Parameter values for this simulation are given in Table A3 of Appendix A.

HbCO levels of 29.5%. The two CO exposure conditions simulated were: (1) short duration (10 min)—high concentration (6462 ppm) and (2) long duration (8 h)—low concentration (265 ppm). The short duration—high concentration simulation would be relevant when victims are trapped for 10 min in a house or closed garage with high CO levels or in a car with its exhaust blocked. The long duration—low concentration simulation would be relevant when there is a faulty furnace at home. Parameters reported for subject 120 of Benignus *et al.*[7] were used for simulating the above two CO exposure conditions. After the end of CO exposure in room air, washout sessions in room air or 100% O_2 for 480 min were simulated. Since MbCO levels and PO_2 in tissues are more reliable indicators of CO toxicity in the tissue, they were estimated for skeletal and myocardial tissue.

Short Duration (10 min)—High Concentration (6462 ppm) CO Exposure

The HbCO levels during short-high CO exposure in room air and washout on air or 100% O_2 are shown in Fig. 8a. Figure 9 shows that even after the end of a short CO exposure, %MbCO continues to increase in the skeletal muscle (~20 and ~35 min in m_1 and m_2, respectively, after end of the CO exposure) as well as cardiac muscle (~1 and ~3 min in c_1 and c_2, respectively, after end of CO exposure) during washout (room air as well as hyperoxia) and then begins to decrease. As shown in Fig. 9, the %MbCO in skeletal ($MbCOm_1$) and myocardial ($MbCOc_1$) muscle tissues peak at higher levels during hyperoxia than during room air washout in the first subcompartments, whereas in the second subcompartments the MbCO ($MbCOm_2$, $MbCOc_2$) levels peak at higher levels during room air washout than during hyperoxia. In hyperoxia, %MbCO is near peak level for a longer time in skeletal muscle. On room air, the MbCO levels are greater in myocardium than in skeletal muscle. With washout in hyperoxia, there is a sudden increase in the MbCO levels in cardiac as well as skeletal muscle. The latter response was also observed in our previously published simulation results.[8–10] In addition, we found that peak MbCO levels occur at different HbCO levels in room air and hyperoxia washout sessions. Peak MbCO levels occur during the CO washout phase with decreasing HbCO levels.

Figures 10a and 10c show the tissue oxygenation in m_1 ($P_{m1}O_2$) and m_2 ($P_{m2}O_2$) during CO exposure and washout in room air. After the end of the short (10 min) CO exposure in room air, $P_{m1}O_2$ decreases by 32.3% from its pre-CO exposure state. In the second subcompartment the tissue PO_2 decreases by 43.8% from its pre-CO exposure state. Figures 10b and 10d show the cardiac muscle tissue PO_2's in c_1 ($P_{c1}O_2$) and c_2 ($P_{c2}O_2$) during CO exposure and washout in room air. After exposure to 6462 ppm CO for 10 min in room air, $P_{c1}O_2$ decreases by 42.2% from its pre-CO exposure state. There is also a large decrease (67.2%) in $P_{c2}O_2$ by the end of the short CO exposure. At the end of the 480 min room air washout session, tissue O_2

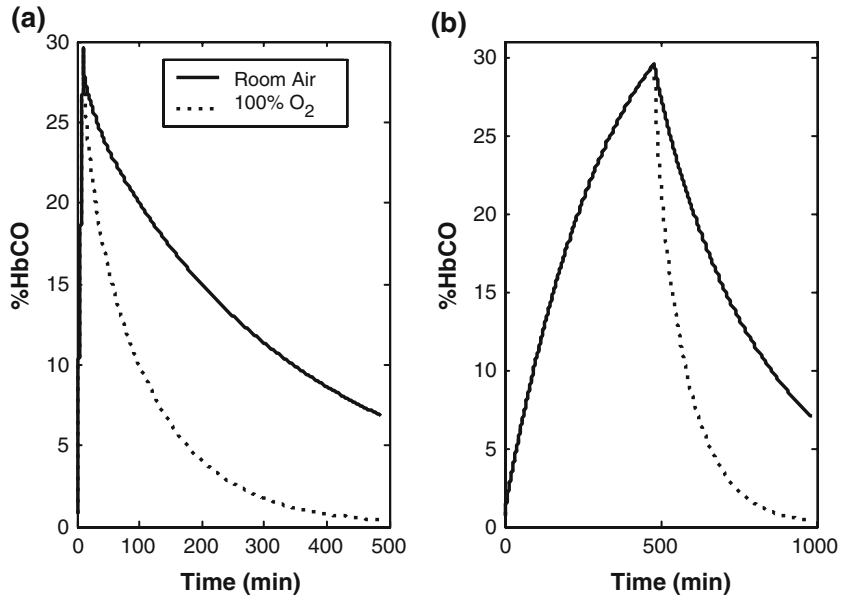

FIGURE 8. Two different CO exposures produce similar HbCO levels at the end of the exposure for subject 120 (from Benignus *et al.*[7]). Comparison of 8 h CO washout from blood on air (*solid line*) and 100% O_2 (*dashed line*) after: (a) short duration, 10 min—high concentration, 6462 ppm, CO exposure in air; (b) long duration, 480 min—low concentration, 265 ppm, CO exposure in air. Parameter values for these simulations are given in Table A3 of Appendix A.

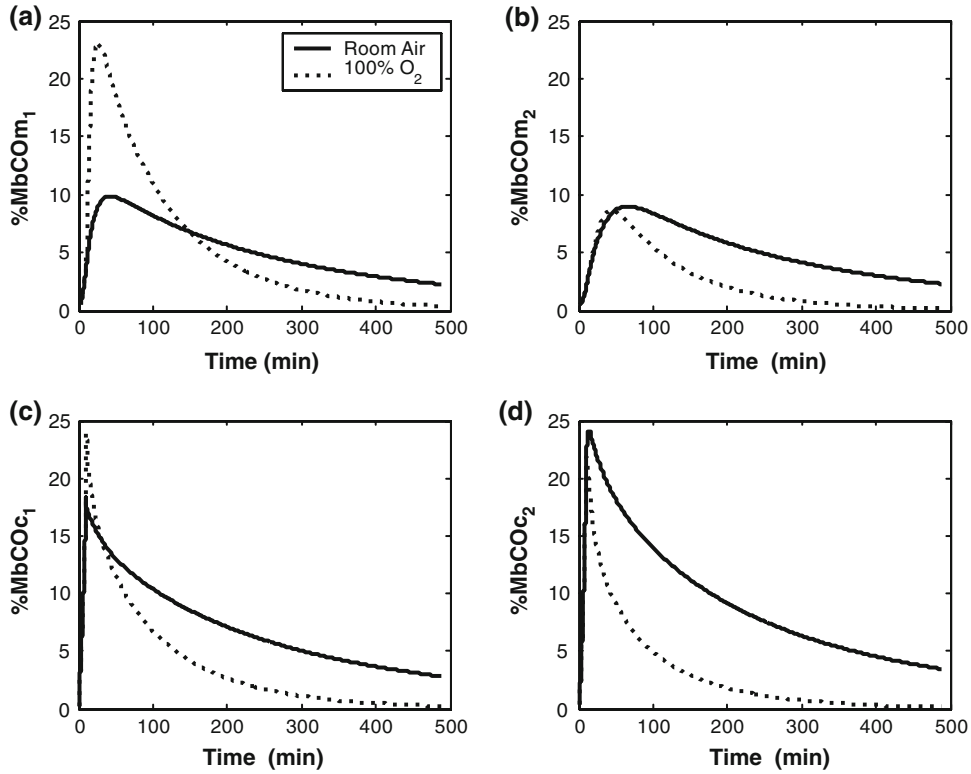

FIGURE 9. Comparison of CO washout on air (*solid line*) and 100% O_2 (*dashed line*) after 10 min exposure to 6462 ppm of CO in air for subject 120 (from Benignus *et al.*[7]). (a, b) MbCO levels of the first (a) and second (b) skeletal muscle tissue subcompartments. (c, d) Myocardial MbCO levels in first subcompartment (c) and second subcompartment (d).

tensions in the skeletal and myocardial subcompartments are still 2–3 Torr below their pre-exposure levels. After the 480 min hyperoxia washout session, the myocardial and skeletal tissue PO_2's are high due to breathing ~100% O_2.

Long Duration (8 h)—Low Concentration (265 ppm) CO Exposure

Figure 8b shows the HbCO levels during an 8-h exposure to 265 ppm CO exposure in room air and washout on air or 100% O_2. Figure 11 shows that after the end of the 8-h CO exposure, %MbCO in the first subcompartments of both the skeletal and the cardiac muscle increases during hyperoxic washout before it begins to decrease. The MbCO levels are higher in the first subcompartments of skeletal and cardiac muscle during hyperoxia when compared to room air. The MbCO levels in the skeletal muscle during washout on room air are similar for both subcompartments. In the cardiac muscle the MbCO levels are greater in the second subcompartment than in the first throughout the course of CO exposure and washout on room air or 100% O_2.

Figures 10c and 10d show the skeletal muscle and myocardial tissue oxygenation in subcompartments 1 and 2 during CO exposure and washout in room air. After the end of a long (8 h) exposure to 265 ppm CO in room air, the tissue PO_2's in m_1 and m_2 decreased by 35.4% and 46.7%, respectively, from their pre-CO exposure values. Myocardial tissue PO_2 in c_1 decreased by 44.9% from its pre-CO exposure state. There is also a large decrease of 66.7% in the tissue PO_2 of c_2 by the end of long CO exposure. The low tissue O_2 tensions of skeletal and cardiac muscle are correlated with the peak MbCO and HbCO levels.

As indicated in Figs. 8–11, although peak HbCO levels are similar for specific long-low and short-high CO exposures, in both tissues (skeletal and cardiac) the MbCO levels at the end of CO exposure as well as the peak MbCO levels are greater after the long-low CO exposure than after the short-high CO exposure. Also, the tissue PO_2's are slightly lower after the long-low CO exposure when compared to the short-high CO exposure. Unlike the short-high CO exposure, in the long-low CO exposure rapid increases in MbCO levels occur only during hyperoxic washout. Figures 12a and 12b show that the total content of CO in the blood at the end of exposure is slightly greater (~4.3%) for the long CO exposure when compared to the short CO exposure even though arterial %HbCO is the same for both exposures. The MbCO levels in both skeletal

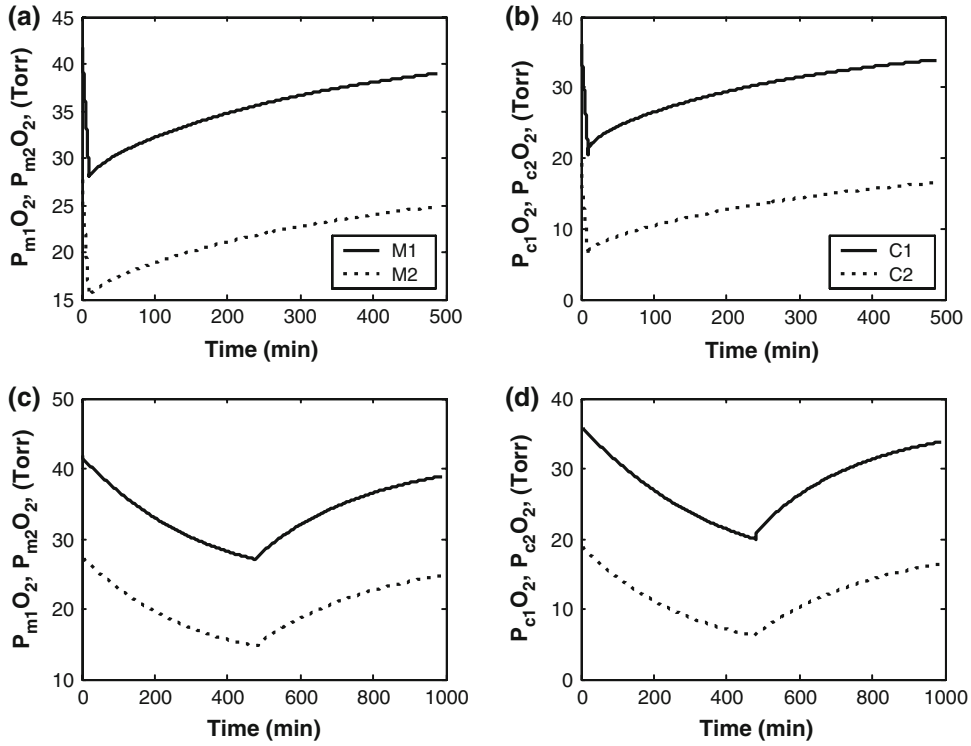

FIGURE 10. Skeletal and cardiac tissue oxygen tension during CO exposure followed by 480 min washout. (a, b) Oxygen tension of the skeletal (a) and myocardial (b) tissues during 10 min exposure to 6462 ppm of CO in air followed by 480 min washout on room air. (c, d) Oxygen tension of the skeletal (c) and myocardial (d) tissues during 480 min exposure to 265 ppm of CO in air followed by 480 min washout on room air. The first subcompartment (*solid line*) and second subcompartment (*dashed line*) oxygen tensions are shown for both skeletal and cardiac tissues for Benignus subject 120.[7] The oxygen tensions in the skeletal and cardiac subcompartments during washout on 100% O_2 reached high values (see text) at the ends of the washout sessions.

muscle subcompartments are greater in the long-low CO exposure than in the short-high CO exposure. At their respective peak MbCO levels, the total CO content in the tissue as seen in Figs. 12c and 12d is greater for the long CO exposure than the short CO exposure (by 42.4% during room air washout and 35.6% during 100% O_2 administration).

The data presented in Fig. 10 demonstrate that at rest, O_2 tensions are greater in skeletal muscle than in myocardial tissue. At the end of CO exposure in room air, the decreases in O_2 tension are larger in the subcompartments of the cardiac muscle than in those of the resting skeletal muscle. The simulations also predict that the second compartments of skeletal and cardiac muscle are more O_2 deprived than the first subcompartments and that tissue PO_2 in the second cardiac subcompartment is approximately one-third of its pre-CO exposure value at the end of CO exposure. Even after 480 min of room air therapy, the O_2 tensions of the skeletal and myocardial tissue do not reach the pre-exposure values. Finally, the low tissue O_2 tensions in skeletal and cardiac muscles are more closely correlated with peak MbCO levels than with the HbCO levels.

Effects of CO Exposure During Exercise

Exercising individuals exposed to CO concentrations higher than the permissible levels are more susceptible to severe tissue hypoxia than those at rest. Because Mb is considered a transient source of O_2 during hypoxic stress and exercise, in the presence of MbCO oxygen availability is reduced.[5,70] In such conditions injury to any exercising muscle, especially the heart, may be severe due to impaired O_2 delivery and temporary unavailability of O_2 stores accompanied by increased O_2 consumption.

Kizakevitch *et al.*[50] conducted experiments involving subjects who exercised during exposure to CO. For each of five levels of HbCO, subjects underwent an experimental protocol comprising rest (R) and three-five-minute treadmill exercise sessions (E1, E2, and E3) with progressively increasing workloads. In this study we simulated experimental sessions at 2% HbCO and 20% HbCO levels. Mean data of three normal subjects (S_{avg}) obtained from the investigators[50] were used for the simulations (Table A3, Appendix A). The MRO_2 at rest for the baseline and 20% HbCO simulation is 180 mL/min. The three exercise sessions for the 2%

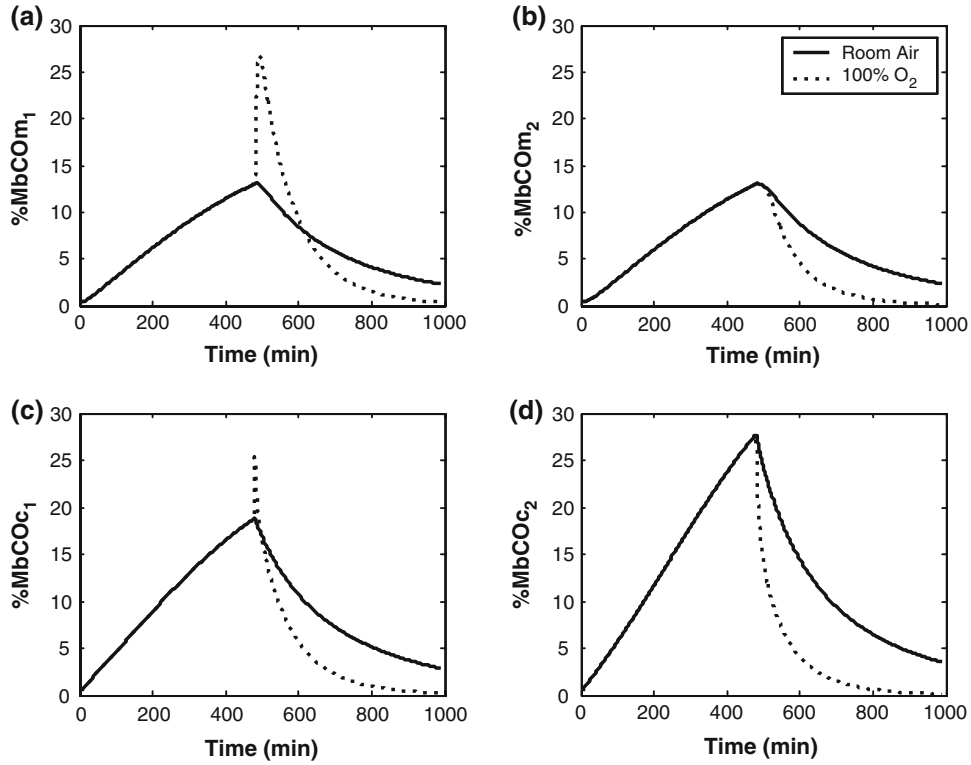

FIGURE 11. Comparison of CO washout on air (*solid line*) and 100% O_2 (*dashed line*) after 480 min exposure to 265 ppm of CO in air for Benignus et al.,[7] subject 120. (a, b) MbCO levels in the first (a) and the second (b) subcompartments of the skeletal muscle. (c, d) MbCO levels in the first (c) and the second (d) subcompartments of the myocardial tissue.

HbCO and 20% HbCO had MRO_2 of 505 mL/min (E1), 690 mL/min (E2), and 931 mL/min (E3). Figure 13 shows the predicted states of oxygenation in the muscle (cardiac and skeletal) tissue and vascular subcompartments during rest and exercise in the presence of CO. The tissue and blood O_2 tensions in the cardiac and skeletal muscle decreased with increasing level of exercise during simulations at baseline HbCO level. There was a further decrease in the tissue as well as blood O_2 tensions of the cardiac and skeletal muscle compartments with increased HbCO level (20%).

DISCUSSION

The deleterious consequences of CO exposure to viability of tissues are mediated through the effects of CO on O_2 delivery and possibly through direct actions of CO on metabolic functions. Uptake of CO by blood can be determined by measuring HbCO levels, whereas uptake of CO by Mb-containing tissues (MbCO levels) and its effects on tissue PO_2 are difficult to measure in CO-poisoned patients. The main objective of this study was to develop a validated model for predicting time varying O_2 tensions and CO levels in human myocardium and skeletal muscle for various CO exposures at rest and during moderate exercise.

Modifications to Our Earlier Model

Skeletal and cardiac muscles exhibit major differences in capillary density, blood flow, and O_2 demand.[8,30,32,43,44,49,65,67] In addition, unlike skeletal muscle, cardiac muscle works constantly. Thus, in contrast to our previous models[8–10] which lump the cardiac muscle with the resting skeletal muscle, the current model has a separate cardiac compartment.

We incorporated two subcompartments instead of a single compartment to represent the heart in order to include arterio-venous shunting and intra-tissue O_2 and CO diffusion. By so doing, we assume subcompartment c_1 to be nearer to the proximal end of arterial supply with entering arterioles, capillaries and exiting venules. Subcompartment c_2 is assumed to be distal to arterioles with gas exchange occurring mainly via capillaries. By making these assumptions, we are attempting to relate the behavior of tissue during CO hypoxia to its distance from an arteriole, a capillary or a venule.[5,33] The MbCO levels and tissue PO_2's in the first compartment would reflect experimental measurements in tissues which lie near an arteriole, while measurements close to a capillary would be comparable to the second subcompartment. Compared to skeletal muscle,[8] the amount of experimental data available for validating the myocardial model with two

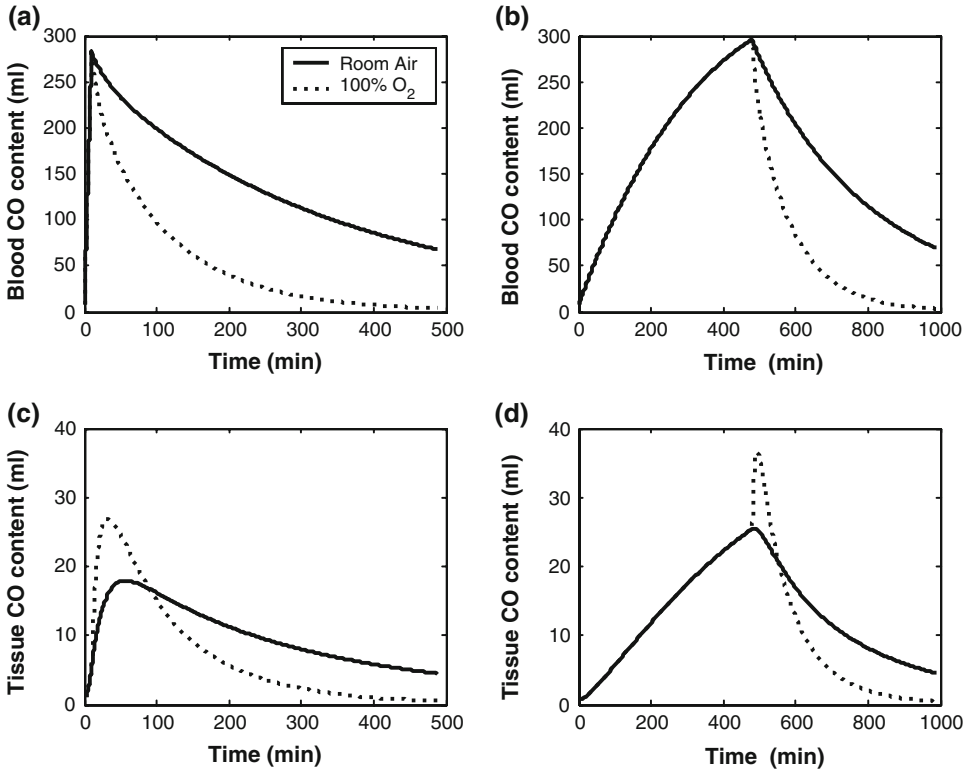

FIGURE 12. Comparison of total CO content in blood and all tissues during CO exposure and washout on air (*solid line*) and 100% O_2 (*dashed line*) for two different CO exposures in air (6462 ppm for 10 min and 265 ppm for 480 min) producing similar HbCO levels at end of the exposure. (a, b) Total content of CO in the blood during (a) high concentration—short duration CO exposure and (b) low concentration—long duration CO exposure. (c, d) Total content of CO in the tissue during (c) high concentration—short duration CO exposure and (d) low concentration—long duration CO exposure.

subcompartments is limited (Table 1). Although absolute values of predicted tissue PO_2's differ somewhat from experimental measurements (Fig. 5), predicted changes in these values relative to changes in arterial PO_2 agree reasonably with the data.

Increase in work load of the heart would result in increased O_2 demand and supply to the heart.[30,43,44,49,65,67] Alterations in these parameters with changing work load were implemented by estimating MOC and MBF as a function of *HR*. Although *HR* is not the best surrogate for MOC and MBF, other indices (e.g., heart rate–blood pressure product, cardiac output) were not available for all of the experimental data used to build the regression relationships. Thus, the current model can simulate conditions of CO exposure during moderate exercise of various intensity levels (which do not cross the anaerobic threshold) but better methods for estimating MOC and MBF are desirable.

Experimentally, *PS* has been found to increase linearly with blood flow (see auxiliary equations in section "Cardiac Muscle Compartment" of Appendix B), contributing to increased diffusive flux of O_2 in times of impaired O_2 delivery.[12] In the model, the effect of vasodilatation and capillary recruitment on blood–tissue gas exchange was implemented by increasing *PS* as a linear function of increases in blood flow to the heart.

In cases where investigators did not measure blood volume in their experiments,[50] blood volume was estimated for individual subjects by means of a regression equation reported in the literature.[56]

Simulation Findings

After validating our model, we analyzed the predicted temporal changes in HbCO levels, MbCO levels, and tissue O_2 tensions in the human myocardium and skeletal muscle for specific CO exposure and washout regimens to obtain insights regarding the potential for hypoxic injury to heart or skeletal muscle tissue. Therefore, we looked for correlations of HbCO and MbCO levels with changes in tissue O_2 tensions for CO exposures of short and long durations and for exercise during CO exposure. Because injury was also reported in CO poisoned victims during therapy,[25,36,50] we also looked for the correlation of HbCO and MbCO levels with tissue O_2 tensions during room air and 100% O_2 breathing following CO exposures.

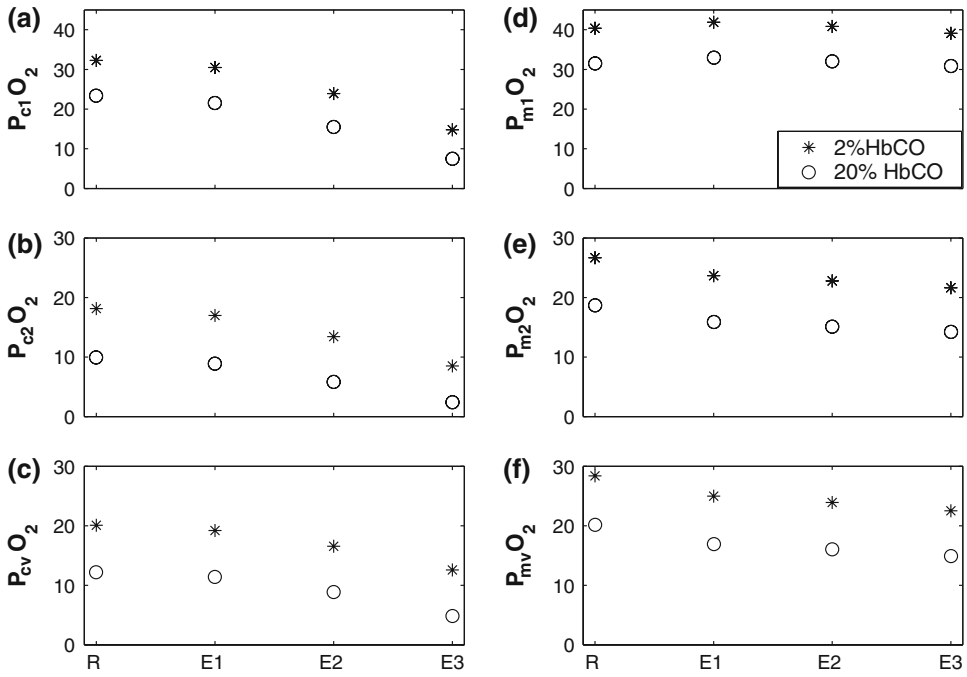

FIGURE 13. Predicted oxygen tensions during treadmill exercise with 2% HbCO (*) and 20% HbCO (○) levels in blood. (a, b) Show the myocardial oxygen tension in tissue subcompartments 1 and 2 ($P_{c_1}O_2$, $P_{c_2}O_2$) during rest (R, and three different stages of exercise (E1, E2, E3). (c) Shows the coronary venous PO_2 ($P_{cv}O_2$) for R, E1, E2, E3. (d–f) Show the tissue ($P_{m_1}O_2$, $P_{m_2}O_2$) and the muscle venous ($P_{mv}O_2$) oxygen tensions for R, E1, E2, E3. Parameter values for these simulations are given in Table A3 of Appendix A.

Myocardium Compared to Skeletal Muscle

Under all of the simulation conditions, the cardiac tissue shows higher MbCO levels and lower tissue O_2 tensions than skeletal muscle. These findings are consistent with the fact that cardiac muscle has a higher O_2 consumption per gram than resting skeletal muscle, although the higher blood flow and capillary density in myocardium partially compensate for its higher O_2 demand. A critical issue is whether the levels of tissue PO_2's predicted in the myocardium represent a potentially injurious limitation of O_2 availability. When PO_2's in myocardial mitochondria drop below 1-2 Torr, oxidative phosphorylation will be impaired, resulting in decreased ATP production.[41,71] We consider a model prediction of tissue $PO_2 < 1$ Torr to be indicative of potential hypoxic injury.[86] The lowest predicted myocardial tissue PO_2 occurs at the end of the third stage of moderate exercise (E3, Fig. 13). With 2% HbCO, $P_{c_2}O_2$ in E3 is well above this threshold for hypoxic injury, but with 20%HbCO $P_{c_2}O_2$ is very near to the level that may impair oxidative phosphorylation.

The risk of hypoxic injury would be greater in subjects exercising during exposure to CO.[57] At the onset of an increase in O_2 demand due to exercise, temporary O_2 deprivation could result because of the reduced storage of O_2 by Mb in the presence of MbCO. Temporary impairment of O_2 delivery to the tissue, together with a decrease in MbO_2 due to an increase in MbCO, could contribute to the observed abnormalities in the ECG and ventricular wall motion in CO poisoned victims.[50] Also, in a patient population with congestive heart failure or coronary artery disease where myocardial perfusion is not normal, exercise during exposure to CO would pose an even greater risk for hypoxic injury for these same reasons.

Our previous models predicted the possibility of injury to muscle tissue during CO exposure. The effect of CO may not be as detrimental to resting skeletal muscle tissue as to exercising skeletal muscle, and both our previous and current simulations may underestimate the potential for injury of skeletal muscle in practical exposure situations. This limitation may apply especially to long CO exposures during moderate to heavy exercise.

From the predictions of our current model we infer that the responses of cardiac muscle and skeletal muscle to CO exposure are qualitatively similar but differ quantitatively due to the anatomical and functional differences between the tissues. In rest and moderate exercise, the myocardium is predicted to be at greater risk for hypoxic injury than skeletal muscle during the course of CO exposure and washout.

Effects of Concentration and Duration of CO Exposure

In our simulations of a short and a long CO exposure, the inspired CO levels were adjusted to produce the same HbCO level (29.5%) at the end of CO exposure in both cases (Fig. 8). Despite this similarity, the MbCO levels and the total content of CO in the blood and tissues at the end of CO exposure are greater for the long CO exposure (Fig. 12). However, the O_2 tensions in both heart and skeletal muscle tissues are only slightly lower at the end of the long exposure than at the end of the short CO exposure.

Our model predicts that the disparities between MbCO responses and HbCO responses occur because CO levels in the blood and tissue do not equilibrate rapidly. MbCO levels in the tissue containing Mb depend on the HbCO levels in the blood, blood flow to the tissue, diffusion coefficient of CO in the tissue, and metabolic demand for O_2 in the tissue. In the short duration–high concentration CO exposure, less CO diffuses from blood into the tissue due to the shorter exposure time and due to the effect of the blood–tissue conductance for CO (which approximately equals that for oxygen).[8] Thus the MbCO levels are lower when compared to the long exposure at low CO concentration (Figs. 9, 10). The rapid increase in HbCO during the short exposure to a high CO concentration results in a greater increase in cardiac output and blood flow to the tissue and, therefore, higher tissue PO_2's when compared to long exposure to a low CO concentration. Of course, during CO exposure and washout regimens, in short as well as long CO exposures, homeostasis requires PO_2's to adjust so that O_2 flux driven by partial pressure gradients will eventually supply adequate O_2 to the tissues.

Washout on Room Air Compared to Washout on 100% O_2

Significant ECG changes, premature ventricular and atrial contractions, congestive heart failure, and fatal arrhythmias have been reported in CO poisoned patients during and after treatment.[25,36,50] In our simulations, MbCO levels in the muscle tissue reached their highest levels during washout on 100% O_2 after CO exposure in room air. Especially in the long-low CO exposure simulation, sharp increases in MbCO levels were observed only during hyperoxia (Fig. 11). Furthermore, the peak MbCO levels were significantly higher during washout on 100% O_2 vs. room air (Figs. 9, 11). The sharp increases in MbCO levels during washout on 100% O_2 suggest that the CO released from Hb by hyperoxia diffuses into tissues and binds to Mb, resulting in elevated MbCO levels in the early part of washout. In washout on 100% O_2, the drop in HbCO is faster due to the higher PaO_2. The increased concentration of dissolved CO in blood increases CO diffusion into the muscle tissue, resulting in higher MbCO levels. During washout on room air, the drop in HbCO level is slower, resulting in less CO being available to diffuse into the muscle. The lower, but longer-lasting, elevation in MbCO levels observed during room air washout when compared to hyperoxia is the result of two competing factors. Hyperoxia displaces more CO from Hb, raising the pressure gradient supporting CO diffusion from blood into tissues. At the same time, exhalation of CO through the lungs is accelerated compared to washout on room air, and the pressure gradient driving CO into tissues is more quickly reversed. Though there is an increase in the MbCO levels with hyperoxia, the tissue was not hypoxic. The tissue O_2 tensions were high because O_2 delivery was enhanced both by the increase in available HbO_2 and by an increase in dissolved O_2 in blood.

Effects of CO Exposure During Exercise

We simulated rest and three different stages of moderate exercise in the presence of 2% HbCO and 20% HbCO. Results (Fig. 13) show that exercise decreases the tissue and blood O_2 tensions in both cardiac and skeletal muscle. Blood and tissue PO_2's in the cardiac compartment are lower at 20% HbCO than at 2% HbCO during rest and the three stages of exercise. The MbCO levels of the cardiac subcompartments increase with exercise, although the HbCO levels are constant. Increased physical activity increases cardiac output which results in increased myocardial work, causing MOC and MBF to increase. Increased MBF increases the CO delivery to the heart and MbCO levels rise. Also, increased myocardial O_2 consumption adds to the prevailing O_2 deficit in the tissue due to CO induced hypoxia. Increased MbCO levels result in decreased MbO_2 levels in the tissue; thus, less O_2 reserve (MbO_2) is available to buffer any further increase in myocardial O_2 consumption until the blood supply to the heart increases. In addition, Mb facilitated diffusion probably contributes to tissue oxygenation over a range of O_2 metabolic demand,[5,86] but this effect has not been implemented in the model. The model prediction of lower myocardial blood and tissue O_2 tensions during exercise in the presence of CO supports the observations of increased risk of cardiac injury in a working population exposed to CO.[50,53,77]

Concerns and Limitations

Parameter Estimation Concerns

For the cardiac compartment, average values from experimental data were considered for most of the

parameters. Predictive equations were developed from data obtained in studies conducted at sea level of healthy Caucasian and African American subjects at rest who ranged in age from 20 to 46 years.

Predictive equations were developed for estimating MBF and MOC. Although more reliable predictions could have been made by calculating the estimates from heart rate–blood pressure product,[43,49,65] blood pressure was not available for the data sets we used.[7,11,50] Estimating MOC and MBF as functions of cardiac output seemed to be an alternative approach, but functional relations among cardiac output, MOC, and MBF could not be found in the literature. Prediction formulas were also used to estimate cardiac output and *HR* based on total body O_2 consumption (Eqs. C.4 and C.6, Appendix C), when actual values were not available. Estimating a value for resting *PS* for the two cardiac subcompartments was very difficult due to unavailability of data. The initial estimates for *PS* were obtained from models[5,12] and then the resting values were scaled to match the size of the tissue, type of the tissue, and the species.

Validation Concerns

The major concern in validating the cardiac compartment of the model was the lack of experimental data from healthy human subjects for testing the model predictions. Consequently, we utilized data predominantly from animal studies. One can see from Table 1 the extent of variability in the data available. Experiments involving swine were emphasized due to the similarity with human coronary anatomy and vasculature.[23,40] Also, most of the data available were from anesthetized animals and the type of anesthesia can have a significant effect.[1,8] Reported values may have a 10–15% error[58] due to O_2 consumption by the electrodes, diffusion of O_2 from blood or tissue to the electrode, and to a shift in electrode position due to beating of the heart. Most of the methods available for measuring myocardial tissue O_2 tension are invasive and insertion of electrodes could have caused damage and bleeding, thereby possibly altering the measured O_2 tensions. As shown in Fig. 5c, model estimates for myocardial vasculature PO_2 correlate well with the experimental coronary venous PO_2. The high degree of reproducibility of experimental coronary venous O_2 tension measurements makes the process of validation easier. On the other hand, the high degree of variability in measurements of myocardial tissue O_2 tension makes the validation of model predictions of tissue PO_2's difficult. The predicted myocardial tissue PO_2's are in agreement with other models[5,31] that utilized a single heart compartment or a distributed (finite-element) model. The predicted capillary blood PO_2 values were also in agreement with mean values reported in Takahashi and Doi.[80]

Concerns Related to Available Experimental Data

In this model, heart rate is required for estimation of myocardial O_2 consumption and blood flow. In the experimental data provided by Benignus *et al.*[7] and Burge and Skinner,[11] heart rate and total body O_2 consumption information were not available. An average whole-body metabolic rate of 0.0032 mL g^{-1} min^{-1} was assumed for all the subjects.[8–10] Total body O_2 consumption, heart rate, myocardial O_2 consumption and blood flow estimated in the model may differ from actual values at the time of experiments. Errors in estimation of the above parameters, especially heart rate, may have significant effects on the model predictions. For simulations of exercise sessions, the CO diffusion coefficient of the lungs (D_LCO) and the pulmonary shunt fraction (SF) are assumed to be constants. Zavorsky *et al.*[88] have reported changes in D_LCO with varying exercise intensity. In addition, the shunt fraction is reported to increase with increases in exercise intensity.[59,79]

Effects of H^+, CO_2, and Lactate

The effects of carbon dioxide (CO_2) and pH on the oxygen dissociation curves (ODC) of hemoglobin and myoglobin have not been included in our simulations. The Bohr and Haldane effects on Hb binding of O_2 might have influenced our model predictions during hypoxia (used during model validation). To examine this issue, we used the polynomial fit equation for calculating P_{50} of Hb (P_{50_Hb}) proposed by Dash and Bassingthwaighte.[19] The P_{50_Hb} was calculated in conditions of normoxia and hypoxia ($F_IO_2 = 0.08$ and 0.06) for the venous measurements of PCO_2 and pH reported by Zhu *et al.*[92] The calculated P_{50_Hb} values during normoxia and the two levels of hypoxic hypoxia were 24.7, 24.9, and 25.5 Torr, respectively. Because the difference in P_{50_Hb} between normoxia and hypoxia was less than one Torr, the Bohr and Haldane effects on the ODC would be small enough to be negligible.

The model presented here is intended to be applied to simulations of rest and mild exercise. Consequently, it has been assumed that several factors which may be important in heavy exercise (i.e., above the lactic acid threshold) are negligible under the conditions we simulated. End-tidal PCO_2 and blood lactate concentration remain near their resting values during exercise at levels below the lactic acid threshold[51] (LAT); therefore, their effects can be ignored if it is shown that our simulated conditions are below the LAT. Blood lactate levels were not measured in the exercise experiments we simulated.[50] Koike *et al.*, reported the total body

O_2 consumption at the LAT ($MRO_{2,L}$) in human subjects (mean age 32.8 years) for no CO exposure and for 20% HbCO.[51] The $MRO_{2,L}$ was 2.26 ± 0.72 L/min for 0% HbCO and 1.75 ± 0.4 L/min for 20% HbCO[51]. In our simulations MRO_2 at the highest exercise level was 0.93 L/min at 2% HbCO and 20% HbCO. Thus, our simulations pertaining to exercise are at levels of O_2 consumption well below the LAT as reported by Koike *et al.*[51]

During exercise, pH decreases and lactate concentration in skeletal muscle tissue increases.[13,24] Both factors can alter the P_{50} of Mb (P_{50_Mb}).[28,75] The lowest pH reported in human skeletal muscle when exercising to fatigue is ~6.5.[45,57] The consequences of changes in pH and lactate concentration on the oxymyoglobin dissociation curve have been determined by assessing their effects on the P_{50_Mb}.[28,75] For intracellular pH values of 6.5, 7.0, or 7.5, the P_{50_Mb} is 2.46, 2.39, and 2.32 Torr, respectively. When we ran our simulation of CO exposure during exercise under the assumption that pH in muscle tissue falls rapidly to 6.5, a level seen only with heavy exercise or ischemia, the tissue PO_2's predicted in skeletal muscle at the end of each 5-min exercise period differed from those reported above only in the second decimal place. Therefore, the decrease in pH associated with moderate exercise would be expected to have only a negligible effect on predicted oxygen tensions.

Lactate accumulation may also alter oxygen binding to Mb.[28] Lactate concentration in resting skeletal muscle fibers is ~2.5 mM, and it can increase to 10 mM in mild to moderate exercise.[13,24] In fatiguing exercise, muscle lactate concentration may rise to 30–40 mM.[13] Increasing lactate concentration 4-fold from 2.5 to 10.0 mM causes P_{50_Mb} to increase by 38%,[28] or from 2.32 to 3.20 Torr in our model. We repeated the simulations of exercise using P_{50_Mb} equal to 10 and found that predicted tissue PO_2's (in both transient and steady state) differed by only tenths of a Torr from those determined with $P_{50\_Mb} = 2.32$. This result is reasonable because the flux of O_2 from blood to tissue is determined by the partial pressure gradient and (in the aerobic steady state, at least) this flux must match the metabolic oxygen consumption. Therefore, the value of P_{50_Mb} has a negligible effect on predicted oxygen tensions (which are our focus). In fatigued skeletal muscles lactate concentrations may rise to 30–40 mM; under such circumstances it would be necessary to adjust the P_{50_Mb} in the model.

Of necessity, the myocardium regulates pH to a much greater extent than does skeletal muscle tissue because cardiac function is impaired by pH changes such that the force of contraction decreases markedly at a pH of 6.8.[63] An abrupt change in pH is adjusted rapidly ("within minutes")[55] in cardiac myocytes by cardiac-specific isoforms of four transporters, carbonic anhydrase, the lactic acid transporter proteins MCT1 and MCT[4,46] and by gap junctions. The heart metabolizes lactate rapidly even at rest, and exercise at 40% of VO_2max does not increase myocardial lactate production.[76] A 4-fold increase in myocardial MRO_2 (more than the increase which occurs in our simulations) is predicted to increase myocardial lactate level from ~3 to ~6 mmol.[90] Furthermore, the presence of CO bound to Mb (as high as 58% MbCO) in the heart does not result in an increase of lactate production over that measured without CO.[16] In addition, simulation studies have demonstrated that increased hydrolysis of ATP in the myocardium activates multiple pathways to support oxidative metabolism.[52,90,91] Indirect evidence based on measuring the ratio of [PCR]/[ATP] and inorganic phosphate (Pi) suggests that any activation of anaerobic metabolism or change in $[H^+]$ at the onset of increased metabolic demand in the myocardium is very short-lived.[35,89] Consequently, it is unlikely that an accumulation of metabolic byproducts in the heart would significantly affect the tissue oxygen tensions predicted in our simulations.

Other Concerns

A primary limitation of the model of cardiac tissues is that it has lumped component parameters. This structure results in the loss of anatomic resolution and functional representation of the tissues. The blood flow, O_2 consumption, capillary density, and O_2 tension vary with layers (epicardium, midmyocardium, endocardium) and chambers of the heart (atria and ventricles). It would be difficult to model all these layers and chambers. Thus, for the purpose of this study, the best choice was to model the region of the left ventricular mid-myocardium because this region is susceptible to injury during CO exposure due to its high O_2 demand. Accordingly, most of the predictive equations for determining blood flow and O_2 consumption were constructed for the left ventricular region (left ventricle and intraventricular septum) of the heart.

CONCLUSION

We developed an improved whole body model capable of predicting the extravascular burden of CO in the human heart and its effects on tissue oxygenation. Determining the CO load on the cardiac tissue allows one to predict O_2 partial pressures within the tissues which are likely to be important predictors of injury. In the current study we have simulated conditions of: (i) transient CO exposure followed by

washout, (ii) hyperoxic rebreathing, (iii) short duration–high concentration CO exposure, (iv) long duration–low concentration CO exposure and (v) CO exposure during moderate exercise. For all the above simulations, we analyzed correlations between HbCO, MbCO, and tissue O_2 tensions to estimate the potential for myocardial and skeletal muscle injury due to CO hypoxia. Although the responses of cardiac muscle and skeletal muscle to CO exposure are qualitatively similar, they differ quantitatively and the myocardium is predicted to be at greater risk for hypoxic injury than skeletal muscle during the course of CO exposure and washout during rest as well as exercise. The current model, which is capable of simulating moderate exercise conditions, suggests that exercising skeletal muscle is more susceptible to injury than resting skeletal muscle during CO exposure. The current model confirms for the myocardium the previous prediction for skeletal muscle[9] that hyperoxic therapy causes an initial rapid increase in MbCO; however, tissue PO_2 levels rise during this time because of the simultaneous rise in P_aO_2. The most serious consequence of an elevated cardiac MbCO may be the diminution of O_2 reserve in the tissue, with the consequence that local O_2 supply may be insufficient to meet a transient increase in metabolic demand. Because the HbCO level in blood is not a reliable indicator of injury, development of this model could prove useful both to estimate risk for hypoxic injury after a CO exposure and to assist in the design of an optimal treatment protocol for a CO-poisoned patient.

Our model was developed to simulate steady state rest and dynamic exercise of moderate intensity during or after sublethal CO exposures (e.g., HbCO $< 30\%$). To simulate conditions of severe hypoxic hypoxia, severe CO hypoxia (e.g., HbCO $> 50\%$), ischemia, prolonged static exercise, or dynamic exercise at MRO_2 levels exceeding the LAT, this model would have to be modified to account for the effects of H^+ and lactate on the oxygen dissociation curves of Hb and Mb.

APPENDIX A: GLOSSARY OF MODEL PARAMETERS AND VARIABLES

This section contains tables of symbols, parameter values, steady state values and initial conditions.

TABLE A1. Primary compartmental variables and parameters.

Symbol	Subscript	Description	Units
C_kO_2		Concentration of O_2 in compartment 'k'	mL/mL
C_kCO		Concentration of CO in compartment 'k'	mL/mL
$COHb_k$		Concentration of CO bound to Hb (HbCO) in compartment 'k'	mL/mL
$COMb_k$		Concentration of CO bound to Mb (MbCO) in compartment 'k'	mL/mL
MR_kO_2		Metabolic rate of O_2 in compartment 'k'	mL/g
O_2Hb_k		Concentration of O_2 bound to hemoglobin (Hb) in compartment 'k'	mL/mL
O_2Mb_k		Concentration of O_2 bound to myoglobin (Mb) in compartment 'k'	mL/mL
P_kO_2		Partial pressure of O_2 in compartment 'k'	Torr
P_kCO		Partial pressure of CO in compartment 'k'	Torr
$\dot{Q}_k$		Blood flow to compartment 'k'	mL/g
V_k		Volume in compartment 'k'	mL

'k'	Description of subscript 'k'
A	Alveolar compartment of lungs
ar	arterial compartment
bc_1	blood compartment 1 of cardiac muscle tissue
bc_2	blood compartment. 2 of cardiac muscle tissue
bc_3 or cv	blood compartment 3 of cardiac muscle tissue
bm_1	blood compartment 1 of skeletal muscle tissue
bm_2	blood compartment 2 of skeletal muscle tissue
bm_3 or mv	blood compartment 3 of skeletal muscle tissue
bot	total blood compartment of other tissue
c	cardiac muscle tissue compartment
c_1	cardiac tissue compartment 1
c_2	cardiac tissue compartment 2
ep	end pulmonary compartment of lungs
ec	end capillary compartment of lungs
I	Inspired gas
m	skeletal muscle tissue compartment

TABLE A1. continued.

'k'	Description of subscript 'k'
m_1	skeletal muscle tissue compartment 1
m_2	skeletal muscle tissue compartment 2
mx	mixed venous compartment
ot	other tissue compartment (nonmuscle)
vot	venous blood compartment of other tissue

TABLE A2. Definition of symbols related to diffusion coefficients and permeability surface area products.

Generic form	Specific parameters	Description
D_kO_2, D_kCO		Diffusion capacity of O_2 or CO in tissue compartment 'k' (mL min^{-1} $Torr^{-1}$)
	D_LO_2, D_LCO	lung diffusion capacity for O_2, CO
	D_MCO	muscle diffusion capacity for CO
Db_kg		Diffusion coefficient of gas 'g' (O_2 or CO) from blood compartment 'k' to tissue compartment (mL min^{-1} $Torr^{-1}$)
	$Db_{c_1}O_2$, $Db_{c_1}CO$	blood (bc_1) to cardiac tissue (c_1)
	$Db_{c_2}O_2$, $Db_{c_2}CO$	blood (bc_2) to cardiac tissue (c_2
	$Db_{c_3}O_2$, $Db_{c_3}CO$	blood (bc_3) to cardiac tissue (c_1)
	$Db_{m_1}O_2$, $Db_{m_1}CO$	blood (bm_1) to muscle tissue (m_1)
	$Db_{m_2}O_2$, $Db_{m_2}CO$	blood (bm_2) to muscle tissue (m_2)
	$Db_{m_3}O_2$, $Db_{m_3}CO$	blood (bm_3) to muscle tissue (m_1)
	$Db_{ot}O_2$, $Db_{ot}CO$	blood (bot) to other tissue (ot)
D'_kg		Intratissue diffusion coefficient of gas 'g' (O_2 or CO) in compartment 'k' (mL min^{-1} $Torr^{-1}$)
	D'_cO_2, D'_cCO	in cardiac subcompartments; c_1, c_2
	D'_mO_2, D'_mCO	in muscle subcompartments; m_1, m_2
PS_sO_2		Permeability surface area product of O_2 for vasculature in compartment 's' (mL min^{-1} $Torr^{-1}$)
	$PS_{c_1}O_2$	for arterioles/venules in cardiac compartment, c_1 ($PS_{cav\_rest}O_2$ is the initial value)
	$PS_{c_2}O_2$	for capillaries in cardiac compartment, c_2 ($PS_{ccap\_rest}O_2$ is the initial value)
	$PS_{m_1}O_2$	for arterioles/venules in muscle compartment, m_1 ($PS_{mav\_rest}O_2$ is the initial value)
	$PS_{m_2}O_2$	for capillaries in muscle compartment, m_2 ($PS_{mcap\_rest}O_2$ is the initial value)

TABLE A3. Definitions of symbols and subject-specific values used in simulation of experiments of Benignus *et al.*[7]; Burge *et al.*,[11] Kizakevich *et al.*[50] (— Indicates "not applicable").

Parameter	Description	Subject 120 of Ref. 7	Subject 2 of Ref. 11	Subject S_{avg}[a] of Ref. 50	Units
Age	Age of the subject	23.9	20	25	years
BW	Body weight of the subject	72.7	63	74.5	kg
C_{Hgb}	Concentration of Hb in blood	0.145	0.1347	0.145	g/mL
CINT	Maximum time step of the integration algorithm	0.001	0.001	0.001	min
COb_0pc	Initial %HbCO level in blood	0.7	2.15	2	none
COm_0pc	Initial %MbCO level in tissue	0.7	2.15	2	none
CO_{ppm}*	Concentration of CO during exposure	6683	13,200	–	ppm
CO_{temp}	Temperature during CO exposure	296	296	296	°Kelvin
D_LCO	Lung diffusion coefficient for CO	29	30	29	mL min^{-1} $Torr^{-1}$
D_MCO	Blood to tissue diffusion coefficient of muscle[8–10]	7	4.5	5	mL min^{-1} $Torr^{-1}$
G	Gender of the subject, G = 0: Female; G = 1: Male	1	0	1	none
HT	Height of the subject	1.791	1.73	1.841	m
O_2INFLOW	O_2 supply to rebreathing circuit	–	230	–	mL/min
$P_{ar}O_2i$	Arterial PO_2 for initial condition	100	640	100	Torr
$P_{B}i$	Barometric pressure for initial condition	760	760	760	Torr
P_mO_2i	Tissue PO_2 for initial condition	21	50	21	Torr
*T*i	End of model initialization time	11.9	11.9	12	min
T_{CO}	Begin time of CO exposure	12	12	–	min
T_{E1}*	Begin time of exercise stage 1, E1	–	–	17	min
T_{E2}*	Begin time of exercise stage 2, E2	–	–	22	min
T_{E3}*	Begin time of exercise stage 3, E3	–	–	27	min
*T*th*	End time of CO exposure and begin time of therapy	17	–	–	min
*T*end*	end time of the simulation	300	52	33	min

TABLE A3. continued.

Parameter	Description	Subject 120 of Ref. 7	Subject 2 of Ref. 11	Subject S_{avg}[a] of Ref. 50	Units
$F_IO_{2\text{-}Ti}$	Fractional inspired O_2 before Ti	0.208	1	0.208	none
$F_IO_{2\text{-}Tco}$	Fractional inspired O_2 after T_{CO}	0.208	1	0.208	none
$F_IO_{2\text{-}Tth}$*	Fractional inspired O_2 after Tth	0.208	–	–	none
HR_{Ti}	HR (heart rate) before Ti	66	66	73	beats/min
HR_{Tco}	HR after T_{CO}	66	66	73	beats/min
HR_{TE1}	HR after T_{E1}	–	–	84.5	beats/min
HR_{TE2}	HR after T_{E2}	–	–	98	beats/min
HR_{TE3}	HR after T_{E3}	–	–	116	beats/min
HR_{Tth}	HR after Tth	66	–	–	beats/min
$MR_{Ti}O_2$	MRO_2 (total body metabolic rate) before Ti	233	224.85	180.5	mL/min
$MR_{Tco}O_2$	MRO_2 after T_{CO}	233	224.85	180.5	mL/min
$MR_{TE1}O_2$	MRO_2 after T_{E1}	–	–	505.15	mL/min
$MR_{TE2}O_2$	MRO_2 after T_{E2}	–	–	690.59	mL/min
$MR_{TE3}O_2$	MRO_2 after T_{E3}	–	–	931.48	mL/min
$MR_{Tth}O_2$	MRO_2 after Tth	233	–	–	mL/min
$\dot{Q}_{Ti}$	$\dot{Q}$(cardiac output) before Ti	5800	Eq. (C.3)	6775	mL/min
$\dot{Q}_{Tco}$	$\dot{Q}$ after T_{CO}	5800	Eq. (C.3)	6775	mL/min
$\dot{Q}_{T_{E1}}$	$\dot{Q}$ after T_{E1}	–	–	11290	mL/min
$\dot{Q}_{T_{E2}}$	$\dot{Q}$ after T_{E2}	–	–	13415	mL/min
$\dot{Q}_{T_{E3}}$	$\dot{Q}$ after T_{E3}	–	–	15570	mL/min
$\dot{Q}_{Tth}$	$\dot{Q}$ after Tth	5800	–	–	mL/min
$Vbperkg$	Volume of blood per kg of BW	60.935	66.24	Eq. (C.2)	mL/kg
$\dot{V}_{Ti}$	Ventilation before Ti ($t \leq Ti$)	5500	6000	3164	mL/min
$\dot{V}_{Tco}$	Ventilation after T_{CO} ($T_{CO} \leq t \leq Tth$)	5500	0	3164	mL/min
$\dot{V}_{T_{E1}}$	Ventilation after T_{E1}	–	–	8860	mL/min
$\dot{V}_{T_{E2}}$	Ventilation after T_{E2}	–	–	10472	mL/min
$\dot{V}_{T_{E3}}$	Ventilation after T_{E3}	–	–	12111	mL/min
$\dot{V}_{Tth}$	Ventilation after Tth ($Tth \leq t \leq Tend$)	6633	–	–	mL/min
V_L	Lung volume	2500	1500[b]	2500	mL

[a]See text in Results section "Effects of CO exposure during Exercise" of the manuscript.
[b]Increases to 5000 mL at $t = Ti$, to account for volume of the rebreathing circuit.
*Values are different for simulations of short-high CO exposure (RA, 100%O_2), long-low CO exposure (RA, 100%O_2), and exercise at 20%HbCO.

TABLE A4. Parameters and their default values.

Parameter	Description and references	Value, units
ρ	Density of muscle[9] tissue	1.04, g/cm^3
C_{Mbc}	Concentration of Mb in cardiac muscle tissue[42]	0.0023, g/mL
C_{Mbm}	Concentration of Mb in skeletal muscle tissue[9]	0.0047, g/mL
D_{bvm_on}	Ratio of $Db_{m3}O_2$ (t) and $Db_{m1}O_2$ (t)[8]	0.075, none
D_{bvc_on}	Ratio of $Db_{c3}O_2$ (t) and $Db_{c1}O_2$ (t)[a]	0.095, none
D_{O_2}	Diffusion coefficient of O_2[9]	0.0006, mL min^{-1} Torr^{-1}
$Db_{ot}O_2$	Diffusion coefficient of O_2 from blood to other tissue (nonmuscle) compartment	7.5, mL min^{-1} Torr^{-1}
dx_m	Mean intercapillary distance in skeletal muscle[9]	0.1, cm
dx_c	Mean intercapillary distance in cardiac muscle[a]	0.0353, cm
F_{vc}	Cardiac muscle tissue volume distribution fraction[a]	0.2, none
F_{vm}	Skeletal muscle tissue volume distribution fraction[8]	0.4, none
K_{O_2}	Oxygen capacity of Hb[9]	1.38, mL O_2/gHb
K_cO_2	PO_2 at which MR_cO_2 decreases by 50%[9]	0.2, Torr
K_mO_2	PO_2 at which MR_mO_2 decreases by 50%[9]	0.5, Torr
M_H	Haldane affinity ratio for hemoglobin (Hb)[9]	218, none
M_M	Haldane affinity ratio for myoglobin (Mb)[9]	36, none
$MR_{am}O_2$	O_2 consumption of arm muscles[8]	0.0014*, mL min^{-1} g^{-1}
$MR_{lm}O_2$	O_2 consumption of leg muscles[8]	0.002*, mL min^{-1} g^{-1}

TABLE A4. continued.

Parameter	Description and references	Value, units
$MR_{tm}O_2$	O_2 consumption of trunk muscles[8]	0.002*, mL min^{-1} g^{-1}
$P_{50}Mb_m$, $P_{50}Mb_c$	Partial pressure of oxygen at 50% of Mb saturation[9] in skeletal (m) and cardiac (c) muscle	2.32, Torr
P_B	Barometric pressure	760, Torr
$PS_{cav\_rest}O_2$	Permeability surface area product of O_2 for arterioles/venules[a] in cardiac muscle	180, mL min^{-1} $Torr^{-1}$ g^{-1}
$PS_{ccap\_rest}O_2$	Permeability surface area product of O_2 for capillaries[a] in cardiac muscle	450, mL min^{-1} $Torr^{-1}$ g^{-1}
$PS_{mav\_rest}O_2$	Permeability surface area product of O_2 for arterioles/venules[8] in skeletal muscle	37.5, mL min^{-1} $Torr^{-1}$ g^{-1}
$PS_{mcap\_rest}O_2$	Permeability surface area product of O_2 for capillaries[8] in skeletal muscle	37.5, mL min^{-1} $Torr^{-1}$ g^{-1}
$\dot{Q}_{amg}$	Blood flow of arm muscles[8]	0.021, mL min^{-1} g^{-1}
$\dot{Q}_{lmg}$	Blood flow of leg muscles[8]	0.03, mL min^{-1} g^{-1}
$\dot{Q}_{tmg}$	Blood flow of trunk muscles[8]	0.03, mL min^{-1} g^{-1}
S_{CO}	Solubility of CO in plasma[9]	2.35×10^{-5}, mL mL^{-1} $Torr^{-1}$
S_{O_2}	Solubility of O_2 in plasma[9]	3.14×10^{-5}, mL mL^{-1} $Torr^{-1}$
SF	Pulmonary shunt fraction[9]	0.02, none
$\dot{V}_A$	Alveolar minute ventilation	5500, mL/min
$\dot{V}_{CO}$	Endogenous CO production[9]	7, μl/min
V_c	Volume of heart[68]	254(M),180(F), mL
V_{iv}	Volume of intra-ventricular septum[68]	64(M), 49(F), mL
V_{lv}	Volume of left ventricle[68]	94(M), 67(F), mL
Vm_0	Normal volume of muscle tissue for 70-kg man[9]	29.1, L
$Volfrac_c$	Fraction of volume of cardiac muscle compartment attributed to blood[48]	0.1161, mL/g
$Volfrac_m$	Fraction of volume of skeletal muscle compartment attributed to blood[9]	0.035, mL/g
$Volfrac_{ot}$	Fraction of volume of other tissue compartment attributed to blood[9]	0.035, mL/g
Vot_0	Normal volume of nonmuscle tissue for 70-kg man[9]	9.6, L

[a]See text in section of the manuscript entitled "Cardiac Compartment Structure and Parameter Estimation".
Values with '' are in STPD and all other values are in BTPS.

TABLE A5. Initial values[a].

Variables	Initial value
$\mathbf{C_AO_2}$	$C_AO_2 = \frac{\mathbf{P_{ar}O_2i}}{\mathbf{P_Bi}}$
$\mathbf{C_ACO}$	$C_ACO = \frac{P_{ar}CO}{\mathbf{P_Bi}}; P_{ar}CO = \frac{\mathbf{P_{ar}O_2i} \cdot COb_0}{(M_H \cdot HbO_2)}; COb_0 = \mathbf{COb_0pc} \cdot \left(\frac{O_2Hb_{max}}{100}\right);$ $HbO_2 = (O_2Hb_{max} - COHb) \cdot \left(\frac{(P)^n}{1+(P)^n}\right); P = \frac{\mathbf{P_{ar}O_2i}}{P_{50}}$
$\mathbf{C_{ar}O_2}$	$C_{ar}O_2 = HbO_2 + (\mathbf{P_{ar}O_2i} \cdot S_{O_2})$
$\mathbf{C_{ar}CO}$	$C_{ar}CO = COb_0$
$\mathbf{C_{m1}O_2}$	$C_{m1}O_2 = \mathbf{P_mO_2i} \cdot S_{O_2} + O_2Mb; O_2Mb = (CMb_{max\,m} - COm_0) \cdot \left(\frac{(P_m)^n}{1+(P_m)^n}\right);$ $C_mO_2 = C_{m1}O_2; COm_0 = \mathbf{COm_0pc} \cdot \left(\frac{CMb_{max}}{100}\right)$
$\mathbf{C_{m1}CO}$	$C_{m1}CO = P_mCO \cdot S_{CO} + COm; P_mCO_0 = \mathbf{P_mO_2i} \cdot \left(\frac{CO_m}{M_M \cdot O_2Mb}\right)$ $CO_m = \frac{COm_0 \cdot CMb_{max\,m}}{100}; P_m = \frac{\mathbf{P_mO_2i}}{P_{50m}}; C_mCO = C_{m1}CO$
$\mathbf{C_{m2}O_2}$	$C_{m2}O_2 = C_mO_2$
$\mathbf{C_{m2}CO}$	$C_{m2}CO = C_mCO$
$\mathbf{C_{mv1}O_2}$	$C_{mv1}O_2 = HbO_2 + (S_{O_2} \cdot \mathbf{P_{ar}O_2i}) - \left(\frac{MR_{m1O_2}}{\dot{Q}_m}\right)$
$\mathbf{C_{mv1}CO}$	$C_{mv1}CO = COb_0$
$\mathbf{C_{mv2}O_2}$	$C_{mv2}O_2 = C_{mv1}O_2 - \left(\frac{MR_{m2O_2}}{\dot{Q}_m}\right)$
$\mathbf{C_{mv2}CO}$	$C_{mv2}CO = COb_0$
$\mathbf{C_{mv3}O_2}$	$C_{mv3}O_2 = C_{mv2}O_2 - 0.5 \cdot \left(\frac{MR_{m2O_2}}{\dot{Q}_m}\right)$
$\mathbf{C_{mv3}CO}$	$C_{mv3}CO = COb_0$
$\mathbf{C_{c1}O_2}$	$C_{c1}O_2 = C_mO_2$
$\mathbf{C_{c1}CO}$	$C_{c1}CO = C_mCO$
$\mathbf{C_{c2}O_2}$	$C_{c2}O_2 = C_mO_2$

TABLE A5. Continued.

Variables	Initial value
$\mathbf{C_{c2}CO}$	$C_{c2}CO = C_mCO$
$\mathbf{C_{cv1}O_2}$	$C_{cv1}O_2 = HbO_2 + (S_{O_2} \cdot \mathbf{P_{ar}O_2i}) - \left(\frac{MR_{c1}O_2}{\dot{Q}_c}\right)$
$\mathbf{C_{cv1}CO}$	$C_{cv1}CO = COb_0$
$\mathbf{C_{cv2}O_2}$	$C_{cv2}O_2 = C_{cv1}O_2 - \left(\frac{MR_{c2}O_2}{\dot{Q}_c}\right)$
$\mathbf{C_{cv2}CO}$	$C_{cv2}CO = COb_0$
$\mathbf{C_{cv3}O_2}$	$C_{cv3}O_2 = C_{cv2}O_2 - 0.5 \cdot \left(\frac{MR_{c2}O_2}{\dot{Q}_c}\right)$
$\mathbf{C_{cv3}CO}$	$C_{cv3}CO = COb_0$
$\mathbf{C_{ot}O_2}$	$P_{ot}O_2 \cdot S_{O_2}; P_{ot}O_{2\_0} = f_{pinv}(HbO_{2vot0}, p50, n, C\max_{ot})$ $HbO_2vot_0 = HbO_2 - \left(\frac{MR_{ot}O_2}{\dot{Q}_{ot}}\right)$
$\mathbf{C_{ot}CO}$	$C_{ot}CO = P_mCO \cdot S_{CO}$
$\mathbf{C_{mx}O_2}$	$C_{mx}O_2 = HbO_2 - 1.1\left(\frac{\mathbf{MRO_2}}{\dot{\mathbf{Q}}}\right)$
$\mathbf{C_{mx}CO}$	$C_{mx}CO = COb_0 + (S_{CO} \cdot P_{mx}CO)$ $P_{mx}CO = \left(\frac{\dot{Q}_m}{\dot{Q}} \cdot P_{mv}CO\right) + \left(\frac{\dot{Q}_c}{\dot{Q}} \cdot P_{cv}CO\right) + \left(\frac{\dot{Q}_{ot}}{\dot{Q}} \cdot P_{vot}CO\right)$

[a]Initial values of variables are calculated from fixed parameter values (Table A4) and user-specified parameters (shown in bold) that depend on the specific study being simulated. See Table A3 for definitions and values of user-specified parameters.

TABLE A6. Steady state values of concentrations (mL/mL) of O_2 (C_kO_2) and CO (C_kCO) for different subjects, whose responses were simulated using values from Table A3.

Variables	Subject 120 of Ref. 7[a]	Subject 2 of Ref. 11[b]	Subject S_{avg} of Ref. 50[c]
C_AO_2	0.153	0.976	0.136
C_ACO	3.08×10^{-6}	3.14×10^{-5}	9.06×10^{-6}
$C_{ep}O_2$	0.197	0.204	0.192
$C_{ep}CO$	1.47×10^{-3}	3.61×10^{-3}	4.11×10^{-3}
$C_{ec}O_2$	0.196	0.203	0.191
$C_{ec}CO$	1.47×10^{-3}	3.61×10^{-3}	4.11×10^{-3}
$C_{ar}O_2$	0.196	0.203	0.191
$C_{ar}CO$	1.47×10^{-3}	3.61×10^{-3}	4.11×10^{-3}
$C_{ot}O_2$	9.28×10^{-4}	9.15×10^{-4}	1.85×10^{-3}
$C_{ot}CO$	6.76×10^{-8}	8.16×10^{-7}	1.89×10^{-7}
$C_{vot}O_2$	0.155	0.141	0.169
$C_{vot}CO$	1.47×10^{-3}	3.62×10^{-3}	4.11×10^{-3}
$C_{m1}O_2$	0.007	0.007	0.007
$C_{m1}CO$	2.41×10^{-5}	1.26×10^{-4}	7.91×10^{-5}
$C_{m2}O_2$	0.006	0.006	0.006
$C_{m2}CO$	2.97×10^{-5}	9.37×10^{-5}	9.54×10^{-5}
$C_{mv1}O_2$	0.128	0.118	0.125
$C_{mv1}CO$	1.48×10^{-3}	3.61×10^{-3}	4.13×10^{-3}
$C_{mv2}O_2$	0.101	0.105	0.101
$C_{mv2}CO$	1.49×10^{-3}	3.70×10^{-3}	4.17×10^{-3}
$C_{mv3}O_2$	0.119	0.127	0.116
$C_{mv3}CO$	1.49×10^{-3}	3.71×10^{-3}	4.17×10^{-3}
$C_{c1}O_2$	4.07×10^{-3}	6.22×10^{-3}	3.89×10^{-3}
$C_{c1}CO$	8.39×10^{-6}	3.64×10^{-5}	2.52×10^{-5}
$C_{c2}O_2$	3.36×10^{-3}	3.47×10^{-3}	3.32×10^{-3}
$C_{c2}CO$	1.02×10^{-5}	2.73×10^{-5}	2.91×10^{-5}
$C_{cv1}O_2$	0.167	0.167	0.167
$C_{cv1}CO$	1.47×10^{-3}	3.61×10^{-3}	4.11×10^{-3}
$C_{cv2}O_2$	0.067	0.068	0.076
$C_{cv2}CO$	1.47×10^{-3}	3.62×10^{-3}	4.11×10^{-3}
$C_{cv3}O_2$	0.069	0.077	0.077
$C_{cv3}CO$	1.47×10^{-3}	3.62×10^{-3}	4.11×10^{-3}
$C_{mx}O_2$	0.147	0.138	0.159
$C_{mx}CO$	1.47×10^{-3}	3.65×10^{-3}	4.11×10^{-3}

[a]Resting, room air.
[b]Resting, 100% O_2.
[c]Resting, room air.

APPENDIX B: MASS BALANCE EQUATIONS FOR OXYGEN (O_2) AND CARBON MONOXIDE (CO)

Lung (Alveolar (L) and End-Pulmonary (ep)) Compartments

$$V_L\frac{dC_AO_2(t)}{dt} = (P_IO_2(t) - P_AO_2(t)) \cdot \frac{\dot{V}_A}{P_B} - O_2flux_{LB}(t) \quad (B.1)$$

$$V_L\frac{dC_ACO(t)}{dt} = (P_ICO(t) - P_ACO(t)) \cdot \frac{\dot{V}_A}{P_B} - COflux_{LB}(t) \quad (B.2)$$

Auxiliary Equations for Lung Compartment

$$P_IO_2 = F_IO_2 \cdot (P_B - 47) \cdot \left(\frac{310}{CO_{temp}}\right)$$

$$P_ICO(t) = \begin{Bmatrix} 0, & 0 \le t < T_{CO} \\ (P_B - 47) \cdot \left(\frac{310}{CO_{temp}}\right) \cdot \left(\frac{CO_{ppm}}{10^6}\right), & T_{CO} \le t < Tth \\ 0, & t \ge Tth \end{Bmatrix}$$

$$O_2flux_{LB}(t) = \dot{Q}(t) \cdot (1 - SF) \cdot \left(C_{ep}O_2(t) - C_{mx}O_2(t - d_v)\right)$$

$$\dot{Q}(t) = \dot{Q}_0 \cdot [1 + 0.572(\%COHb(t))]$$

If $\dot{Q}_0$ is not measured by the investigators then regression equations (Eqs. C.3 or C.4) are used to estimate $\dot{Q}_0$.

$$C_{ep}O_2(t) = O_2Hb_{ep}(t) + S_{O_2} \cdot P_{ep}O_2(t)$$

$$O_2Hb_{ep}(t) = f_{odc}(P_{ep}O_2(t), P_{50}(t), n(t), C_{maxep}(t))$$

[See section "Special Functions" (F.1) for description of f_{odc}]

$$P_{ep}O_2(t) = P_AO_2(t)$$

$$P_AO_2(t) = C_AO_2(t) \cdot P_B$$

$$P_{50}(t) = 50.4219[1 + \exp\{0.0215(\%COHb(t))\}]^{-1}$$

$$n(t) = 1.7493 + 0.5909[\exp\{-0.025(\%COHb(t))\}]$$

$$\%COHb(t) = \left(\frac{100 \cdot COHb(t)}{O_2Hb_{max}}\right)$$

$$COHb(t) = C_{ar}CO(t) - (S_{CO} \cdot P_{ar}CO(t))$$

$$C_{maxep}(t) = O_2Hb_{max} - COHb_{ep}(t)$$

$$O_2Hb_{max} = K_{O_2}(C_{Hgb})$$

$$COHb_{ep}(t) = C_{ep}CO(t) - \left(S_{CO} \cdot P_{ep}CO(t)\right)$$

$$C_{ep}CO(t) = C_{mx}CO(t - d_v) + \left(\frac{COflux_{LB}(t)}{(1 - SF) \cdot \dot{Q}(t)}\right)$$

$$C_{mx}CO(t) = COHb_{mx}(t) + (S_{CO} \cdot P_{mx}CO(t))$$

[See section "Mixed Venous Blood Compartment, (mx)" for definition of $COHb_{mx}(t)$]

$$COflux_{LB}(t) = \left[P_ACO - 0.5\left(P_{ep}CO(t) + P_{mx}CO(t - d_v)\right)\right] \cdot D_LCO$$

$$P_ACO(t) = C_ACO(t) \cdot P_B$$

$$P_{ep}CO(t) = \left(\frac{P_{ep}O_2(t)}{M_H}\right) \cdot \left(\frac{COHb_{ep}(t)}{O_2Hb_{ep}(t)}\right)$$

Lung (End-Capillary) Compartment, (ec)

$$C_{ec}O_2(t) = SF \cdot C_{mx}O_2(t - d_v) + (1 - SF) \cdot C_{ep}O_2(t)$$

$$O_2Hb_{ec}(t) = f_{odc}(P_{ec}O_2(t), P_{50}(t), n(t), C_{maxec}(t))$$

[See section "Special Functions" (F.1) for description of f_{odc}]

$$P_{ec}O_2(t) = f_{imp}(S_{O_2}, C_{maxec}(t), P_{50}(t), n(t), C_{ec}O_2(t))$$

[See section "Special Functions" (F.3) for description of f_{imp}]

$$C_{maxec}(t) = O_2Hb_{max} - COHb_{ec}(t)$$

$$COHb_{ec}(t) = C_{ec}CO(t) - S_{CO} \cdot P_{ec}CO(t)$$

$$C_{ec}CO(t) = C_{mx}CO(t - d_v) + \frac{COflux_{LB}(t)}{\dot{Q}(t)}$$

$$P_{ec}CO(t) = \left(\frac{P_{ec}O_2(t)}{M_H}\right) \cdot \left(\frac{COHb_{ec}(t)}{O_2Hb_{ec}(t)}\right)$$

Arterial Blood Compartment, (ar)

$$V_{ar}\frac{dC_{ar}O_2(t)}{dt} = (C_{ec}O_2(t) - C_{ar}O_2(t)) \cdot \dot{Q}(t) \quad (B.3)$$

$$V_{ar}\frac{dC_{ar}CO(t)}{dt} = (C_{ec}CO(t) - C_{ar}CO(t)) \cdot \dot{Q}(t) \quad (B.4)$$

Auxiliary Equations for Arterial Blood Compartment

$$\mathrm{P_{ar}O_2}(t) = f_{\mathrm{imp}}(\mathrm{S_{O_2}}, C_{\mathrm{maxar}}(t), \mathrm{P_{50}}(t), n(t), C_{\mathrm{ar}}\mathrm{O_2}(t))$$

[See section "Special Functions" (F.3) for description of f_{imp}]

$$C_{\mathrm{maxar}}(t) = \mathrm{O_2Hb_{max}} - \mathrm{COHb}(t)$$

$$\mathrm{O_2Hb_{ar}}(t) = f_{\mathrm{odc}}(\mathrm{P_{ar}O_2}(t), \mathrm{P_{50}}(t), n(t), C_{\mathrm{maxar}}(t))$$

[See section "Special Functions" (F.1) for description of f_{odc}]

$$\mathrm{P_{ar}CO}(t) = \left(\frac{\mathrm{P_{ar}O_2}(t)}{M_{\mathrm{H}}}\right) \cdot \left(\frac{\mathrm{COHb}(t)}{\mathrm{O_2Hb_{ar}}(t)}\right)$$

$$V_{\mathrm{ar}} = 0.25(V_{\mathrm{b}} - V_{\mathrm{bm}} - V_{\mathrm{bot}})$$

Skeletal Muscle Compartment

Skeletal Muscle Tissue Compartment 1, (m_1)

$$\frac{dC_{\mathrm{m1}}\mathrm{O_2}(t)}{dt} = \frac{\mathrm{Flux_{m1}O_2}(t)}{V_{\mathrm{m1}}} + \frac{D'_{\mathrm{m}}\mathrm{O_2} \cdot \left(C^d_{\mathrm{m2}}\mathrm{O_2}(t) - C^d_{\mathrm{m1}}\mathrm{O_2}(t)\right)}{D_{\mathrm{xm}}} - \frac{MR_{\mathrm{m1}}\mathrm{O_2}(t)}{V_{\mathrm{m1}}} \tag{B.5}$$

$$\frac{dC_{\mathrm{m1}}\mathrm{CO}(t)}{dt} = \frac{\mathrm{Flux_{m1}CO}(t)}{V_{\mathrm{m1}}} + \frac{D'_{\mathrm{m}}\mathrm{CO} \cdot \left(C^d_{\mathrm{m2}}\mathrm{CO}(t) - C^d_{\mathrm{m1}}\mathrm{CO}(t)\right)}{D_{\mathrm{xm}}} \tag{B.6}$$

Skeletal Muscle Tissue compartment 2, (m_2)

$$\frac{dC_{\mathrm{m2}}\mathrm{O_2}(t)}{dt} = \frac{\mathrm{Flux_{m2}O_2}(t)}{V_{\mathrm{m2}}} + \frac{D'_{\mathrm{m}}\mathrm{O_2} \cdot \left(C^d_{\mathrm{m1}}\mathrm{O_2}(t) - C^d_{\mathrm{m2}}\mathrm{O_2}(t)\right)}{D_{\mathrm{xm}} \cdot \left(V_{\mathrm{m2}}/V_{\mathrm{m1}}\right)} - \frac{MR_{\mathrm{m2}}\mathrm{O_2}(t)}{V_{\mathrm{m2}}} \tag{B.7}$$

$$\frac{dC_{\mathrm{m2}}\mathrm{CO}(t)}{dt} = \frac{\mathrm{Flux_{m2}CO}(t)}{V_{\mathrm{m2}}} + \frac{D'_{\mathrm{m}}\mathrm{CO} \cdot \left(C^d_{\mathrm{m1}}\mathrm{CO}(t) - C^d_{\mathrm{m2}}\mathrm{CO}(t)\right)}{D_{\mathrm{xm}} \cdot \left(V_{\mathrm{m2}}/V_{\mathrm{m1}}\right)} \tag{B.8}$$

Skeletal Blood compartment 1, (bm_1)

$$V_{\mathrm{bm1}}\frac{dC_{\mathrm{mv1}}\mathrm{O_2}(t)}{dt} = \dot{Q}_{\mathrm{m}}(t) \cdot (C_{\mathrm{ar}}\mathrm{O_2}(t) - C_{\mathrm{mv1}}\mathrm{O_2}(t)) - \mathrm{O_2Flux_{m1}}(t) \tag{B.9}$$

$$V_{\mathrm{bm1}}\frac{dC_{\mathrm{mv1}}\mathrm{CO}(t)}{dt} = \dot{Q}_{\mathrm{m}}(t) \cdot (C_{\mathrm{ar}}\mathrm{CO}(t) - C_{\mathrm{mv1}}\mathrm{CO}(t)) - \mathrm{COFlux_{m1}}(t) \tag{B.10}$$

Skeletal Blood compartment 2, (bm_2):

$$V_{\mathrm{bm2}}\frac{dC_{\mathrm{mv2}}\mathrm{O_2}(t)}{dt} = \dot{Q}_{\mathrm{m}}(t) \cdot (C_{\mathrm{mv1}}\mathrm{O_2}(t) - C_{\mathrm{mv2}}\mathrm{O_2}(t)) - \mathrm{O_2Flux_{m2}}(t) \tag{B.11}$$

$$V_{\mathrm{bm2}}\frac{dC_{\mathrm{mv2}}\mathrm{CO}(t)}{dt} = \dot{Q}_{\mathrm{m}}(t) \cdot (C_{\mathrm{mv1}}\mathrm{CO}(t) - C_{\mathrm{mv2}}\mathrm{CO}(t)) - \mathrm{COFlux_{m2}}(t) \tag{B.12}$$

Skeletal Blood compartment 3, (bm_3):

$$V_{\mathrm{bm3}}\frac{dC_{\mathrm{mv3}}\mathrm{O_2}(t)}{dt} = \dot{Q}_{\mathrm{m}}(t) \cdot (C_{\mathrm{mv2}}\mathrm{O_2}(t) - C_{\mathrm{mv3}}\mathrm{O_2}(t)) - \mathrm{O_2Flux_{m3}}(t) \tag{B.13}$$

$$V_{\mathrm{bm3}}\frac{dC_{\mathrm{mv3}}\mathrm{CO}(t)}{dt} = \dot{Q}_{\mathrm{m}}(t) \cdot (C_{\mathrm{mv2}}\mathrm{CO}(t) - C_{\mathrm{mv3}}\mathrm{CO}(t)) - \mathrm{COFlux_{m3}}(t) \tag{B.14}$$

Auxiliary Equations for Skeletal Tissue Compartment 1, m_1

$$V_{\mathrm{m1}} = Fv_{\mathrm{m}} \cdot V_{\mathrm{m}}$$

$$MR_{\mathrm{m1}}\mathrm{O_2} = (MR_{\mathrm{m}}\mathrm{O_2}) \cdot \frac{V_{\mathrm{m1}}}{V_{\mathrm{m1}} + V_{\mathrm{m2}}}$$

$$MR_{\mathrm{m}}\mathrm{O_2} = 1.21\left(\frac{MR_{\mathrm{lm}}\mathrm{O_2} \cdot V_{\mathrm{lm}} + MR_{\mathrm{am}}\mathrm{O_2} \cdot V_{\mathrm{am}} + MR_{\mathrm{tm}}\mathrm{O_2} \cdot V_{\mathrm{tm}}}{\rho}\right)$$

$$MR_{\mathrm{m1}}\mathrm{O_2}(t) = (MR_{\mathrm{m}}\mathrm{O_2}) \cdot \left(\frac{V_{\mathrm{m1}}}{V_{\mathrm{m1}} + V_{\mathrm{m2}}}\right) \cdot \left(\frac{\mathrm{P_{m1}O_2}(t)}{K_{\mathrm{m}}\mathrm{O_2} + \mathrm{P_{m1}O_2}(t)}\right)$$

$$\mathrm{Flux_{m1}O_2}(t) = \mathrm{O_2Flux_{m1}}(t) + \mathrm{O_2Flux_{m3}}(t)$$

$$\mathrm{P_{m1}O_2}(t) = f_{\mathrm{imp}}(\mathrm{S_{O_2}}, \mathrm{O_2Mb_{maxm1}}(t), \mathrm{P_{50m}}, C_{\mathrm{m1}}\mathrm{O_2}(t), V_{\mathrm{m1}})$$

[See section "Special Functions" (F.3) for description of f_{imp}]

$$C^{d}_{\mathrm{m1}}\mathrm{O_2}(t) = C_{\mathrm{m1}}\mathrm{O_2}(t) - \mathrm{O_2Mb_{m1}}(t)$$

$$C^{d}_{\mathrm{m1}}\mathrm{CO}(t) = \mathrm{S_{CO}} \cdot \mathrm{P_{m1}CO}(t)$$

$$\mathrm{O_2Mb_{maxm1}}(t) = C\mathrm{Mb_{max}} - \mathrm{COMb_{m1}}(t)$$

$$C\mathrm{Mb_{max}} = \frac{64500}{17000}\left(\frac{K_{\mathrm{O_2}}}{4} \cdot C_{\mathrm{Mbm}}\right)$$

$$\mathrm{COMb_{m1}}(t) = C_{\mathrm{m1}}\mathrm{CO}(t) - (\mathrm{S_{CO}} \cdot \mathrm{P_{m1}CO}(t))$$

$$\mathrm{P_{m1}CO}(t) = \left(\frac{\mathrm{P_{m1}O_2}(t)}{M_{\mathrm{M}}}\right) \cdot \left(\frac{\mathrm{COMb_{m1}}(t)}{\mathrm{O_2Mb_{m1}}(t)}\right)$$

$$\mathrm{O_2Mb_{m1}}(t) = \mathrm{O_2Mb_{maxm1}}(t) \cdot \left(\frac{\mathrm{P_{m1}O_2}(t)}{\mathrm{P_{50m}} + \mathrm{P_{m1}O_2}(t)}\right)$$

$$D^{'}_{\mathrm{m}}\mathrm{O_2} = 600 \cdot D\mathrm{O_2}$$

$$\mathrm{Flux_{m1}CO}(t) = \mathrm{COFlux_{m1}}(t) + \mathrm{COFlux_{m3}}(t)$$

$$D^{'}_{\mathrm{m}}\mathrm{CO} = 0.75 D^{'}_{\mathrm{m}}\mathrm{O_2}$$

$$C_{\mathrm{m1}}\mathrm{O_2}(t) = \mathrm{O_2Mb_{m1}}(t) + \mathrm{S_{O_2}} \cdot \mathrm{P_{m1}O_2}(t)$$

$$C_{\mathrm{m1}}\mathrm{CO}(t) = \mathrm{COMb_{m1}}(t) + \mathrm{S_{CO}} \cdot \mathrm{P_{m1}CO}(t)$$

Auxiliary Equations for Skeletal Tissue Compartment 2, m_2

$$V_{\mathrm{m2}} = (1 - Fv_{\mathrm{m}}) \cdot V_{\mathrm{m}}$$

$$MR_{\mathrm{m2}}\mathrm{O_2} = (MR_{\mathrm{m}}\mathrm{O_2}) \cdot \frac{V_{\mathrm{m2}}}{V_{\mathrm{m1}} + V_{\mathrm{m2}}}$$

$$\mathrm{Flux_{m2}O_2}(t) = \mathrm{O_2Flux_{m2}}(t)$$

$$\mathrm{Flux_{m2}CO}(t) = \mathrm{COFlux_{m2}}(t)$$

$$C^{d}_{\mathrm{m2}}\mathrm{O_2}(t) = C_{\mathrm{m2}}\mathrm{O_2}(t) - \mathrm{O_2Mb_{m2}}(t)$$

$$C^{d}_{\mathrm{m2}}\mathrm{CO}(t) = \mathrm{S_{CO}} \cdot \mathrm{P_{m2}CO}(t)$$

All other equations are similar to those of skeletal tissue compartment 1.

Auxiliary Equations for Skeletal Blood Compartment 1, (bm_1)

$$\mathrm{O_2Flux_{m1}}(t) = D\mathrm{b_{m1}O_2}(t) \cdot (\mathrm{P_{a1m}O_2}(t) - \mathrm{P_{m1}O_2}(t))$$

$$\mathrm{P_{a1m}O_2}(t) = f_{\mathrm{getPavg}}\big(\mathrm{O_2Hb_{maxm1}}(t), V\mathrm{b_{m1}}, \mathrm{P_{50}}(t), n(t), C_{\mathrm{m1av}}\mathrm{O_2}(t), \mathrm{S_{O_2}}, \mathrm{P_{ar}O_2}(t), \mathrm{P_{mv1}O_2}(t)\big)$$

[See section "Special Functions" (F.5) for description of f_{getPavg}]

$$\mathrm{O_2Hb_{maxm1}}(t) = \mathrm{O_2Hb_{max}} - \mathrm{COHb}(t)$$

$$C_{\mathrm{m1av}}\mathrm{O_2}(t) = 0.5(C_{\mathrm{ar}}\mathrm{O_2}(t) + C_{\mathrm{mv1}}\mathrm{O_2}(t))$$

$$\dot{Q}_{\mathrm{m}}(t) = \dot{Q}_{\mathrm{m0}} \cdot [1 + 0.572(\%\mathrm{COHb}(t))]$$

$$\dot{Q}_{\mathrm{m0}} = (\dot{Q}_{\mathrm{lmg}} \cdot V_{\mathrm{lm}}) + (\dot{Q}_{\mathrm{amg}} \cdot V_{\mathrm{am}}) + (\dot{Q}_{\mathrm{tmg}} \cdot V_{\mathrm{tm}})$$

$$V_{\mathrm{bm1}} = F_{\mathrm{vm}} \cdot V_{\mathrm{bm}}$$

$$V_{\mathrm{bm}} = \mathrm{volfrac_m} \cdot V_{\mathrm{m}}$$

$$[\mathrm{P_{mv1}O_2}(t), \mathrm{O_2Hb_{mv1}}(t)] = f_{\mathrm{getPO_2}}(\mathrm{O_2Hb_{ar}}(t), \mathrm{P_{50}}(t), n(t), \mathrm{O_2Hb_{max\,m1}}(t), S_{\mathrm{O_2}}, \mathrm{P_{ar}O_2}(t), \dot{Q}_{\mathrm{m}}(t))$$

[See section "Special Functions" (F.4) for description of $f_{\mathrm{getPO_2}}$]

$$D\mathrm{b_{m1}O_2}(t) = \frac{PS_{\mathrm{m1}}\mathrm{O_2}(t) \cdot \mathrm{S_{O_2}} \cdot V_{\mathrm{m1}}}{1.04}$$

$$PS_{\mathrm{m1}}\mathrm{O_2}(t) = PS_{\mathrm{mav\_rest}} \cdot \frac{\dot{Q}_{\mathrm{m}}(t)}{\dot{Q}_{\mathrm{m0}}}$$

$$\mathrm{COFlux_{m1}}(t) = D\mathrm{b_{m1}CO}(t) \cdot (\mathrm{P_{a1m}CO}(t) - \mathrm{P_{m1}CO}(t))$$

$$D_{\mathrm{bm1}}\mathrm{CO}(t) = D_{\mathrm{M}}\mathrm{CO} \cdot \left(\frac{D\mathrm{b_{m1}O_2}(t)}{D\mathrm{b_{m2}O_2}(t)}\right)$$

$$\mathrm{P_{a1m}CO}(t) = 0.5(\mathrm{P_{ar}CO}(t) + \mathrm{P_{mv1}CO}(t))$$

$$\mathrm{P_{mv1}CO}(t) = \left(\frac{\mathrm{P_{mv1}O_2}(t)}{M_{\mathrm{H}}}\right) \cdot \left(\frac{\mathrm{COHb_{mv1}}(t)}{\mathrm{O_2Hb_{mv1}}(t)}\right)$$

$$\mathrm{COHb_{mv1}}(t) = C_{\mathrm{mv1}}\mathrm{CO}(t) - (\mathrm{S_{CO}} \cdot \mathrm{P_{mv1}CO}(t))$$

Auxiliary Equations for Skeletal Blood Compartment 2, (bm_2)

$$\mathrm{O_2Flux_{m2}}(t) = D\mathrm{b_{m2}O_2}(t) \cdot (\mathrm{P_{a2m}O_2}(t) - \mathrm{P_{m2}O_2}(t))$$

$$V_{\mathrm{bm2}} = (1 - F_{\mathrm{vm}}) \cdot V_{\mathrm{bm}}$$

$$D\mathrm{b_{m2}O_2}(t) = \frac{PS_{\mathrm{m2}}\mathrm{O_2}(t) \cdot \mathrm{S_{O_2}} \cdot V_{\mathrm{m2}}}{1.04}$$

$$PS_{m2}O_2(t) = PS_{mcap\_rest} \cdot \frac{\dot{Q}_m(t)}{\dot{Q}_{m0}}$$
$$COFlux_{m2}(t) = Db_{m2}CO(t) \cdot (P_{a2m}CO(t) - P_{m2}CO(t))$$
$$Db_{m2}CO(t) = D_MCO$$

All other equations are similar to those of skeletal blood compartment 1.

Auxiliary Equations for Skeletal Blood Compartment 3, (bm_3)

$$O_2Flux_{m3}(t) = Db_{m3}O_2(t) \cdot (P_{a3m}O_2(t) - P_{m1}O_2(t))$$
$$V_{bm3} = D_{bvm\_on} \cdot V_{bm1}$$
$$Db_{m3}O_2(t) = Db_{m1}O_2(t) \cdot D_{bvm\_on}$$
$$COFlux_{m3}(t) = D_{bm3}CO(t) \cdot (P_{a3m}CO(t) - P_{m1}CO(t))$$
$$D_{bm3}CO(t) = D_MCO \cdot \left(\frac{Db_{m3}O_2(t)}{Db_{m2}O_2(t)}\right)$$

All other equations are similar to those of skeletal blood compartment 1.

Cardiac Muscle Compartment

Cardiac Muscle Tissue Compartment 1, (c_1)

$$\frac{dC_{c1}O_2(t)}{dt} = \frac{Flux_{c1}O_2(t)}{V_{c1}} + \frac{D_c'O_2 \cdot \left[C_{c2}^dO_2(t) - C_{c1}^dO_2(t)\right]}{D_{xc}} - \frac{MR_{c1}O_2(t)}{V_{c1}} \quad \text{(B.15)}$$

$$\frac{dC_{c1}CO(t)}{dt} = \frac{Flux_{c1}CO(t)}{V_{c1}} + \frac{D_c'CO \cdot \left[C_{c2}^dCO(t) - C_{c1}^dCO(t)\right]}{D_{xc}} \quad \text{(B.16)}$$

Cardiac Muscle Tissue Compartment 2, (c_2)

$$\frac{dC_{c2}O_2(t)}{dt} = \frac{Flux_{c2}O_2(t)}{V_{c2}} + \frac{D_c'O_2 \cdot \left(C_{c1}^dO_2(t) - C_{c2}^dO_2(t)\right)}{D_{xc} \cdot \left(V_{c2}/V_{c1}\right)} - \frac{MR_{c2}O_2(t)}{V_{c2}} \quad \text{(B.17)}$$

$$\frac{dC_{c2}CO(t)}{dt} = \frac{Flux_{c2}CO(t)}{V_{c2}} + \frac{D_c'CO \cdot \left(C_{c1}^dCO(t) - C_{c2}^dCO(t)\right)}{D_{xc} \cdot \left(V_{c2}/V_{c1}\right)} \quad \text{(B.18)}$$

Cardiac Blood compartment 1, (bc_1)

$$V_{bc1}\frac{dC_{cv1}O_2(t)}{dt} = \dot{Q}_c(t) \cdot (C_{ar}O_2(t) - C_{cv1}O_2(t)) - O_2Flux_{c1}(t) \quad \text{(B.19)}$$

$$V_{bc1}\frac{dC_{cv1}CO(t)}{dt} = \dot{Q}_c(t) \cdot (C_{ar}CO(t) - C_{cv1}CO(t)) - COFlux_{c1}(t) \quad \text{(B.20)}$$

Cardiac Blood compartment 2, (bc_2)

$$V_{bc2}\frac{dC_{cv2}O_2(t)}{dt} = \dot{Q}_c(t) \cdot (C_{cv1}O_2(t) - C_{cv2}O_2(t)) - O_2Flux_{c2}(t) \quad \text{(B.21)}$$

$$V_{bc2}\frac{dC_{cv2}CO(t)}{dt} = \dot{Q}_c(t) \cdot (C_{cv1}CO(t) - C_{cv2}CO(t)) - COFlux_{c2}(t) \quad \text{(B.22)}$$

Cardiac Blood compartment 3, (c_3)

$$V_{bc3}\frac{dC_{cv3}O_2(t)}{dt} = \dot{Q}_c(t) \cdot (C_{cv2}O_2(t) - C_{cv3}O_2(t)) - O_2Flux_{c3}(t) \quad \text{(B.23)}$$

$$V_{bc3}\frac{dC_{cv3}CO(t)}{dt} = \dot{Q}_c(t) \cdot (C_{cv2}CO(t) - C_{cv3}CO(t)) - COFlux_{c3}(t) \quad \text{(B.24)}$$

Auxiliary Equations Cardiac Tissue Compartment 1, c_1

$$V_{c1} = Fv_c \cdot V_c$$
$$MR_{c1}O_2 = (MR_cO_2) \cdot \frac{V_{c1}}{V_{c1} + V_{c2}}$$
$$MR_cO_2 = 1.21\left(\frac{M_c \cdot V_c}{100\rho}\right)$$
$$M_c = \frac{46.6}{1 + \left(\frac{122.7}{HR}\right)^{4.85}} + 9.76$$
$$MR_{c1}O_2(t) = (MR_cO_2) \cdot \left(\frac{V_{c1}}{V_{c1} + V_{c2}}\right) \cdot \left(\frac{P_{c1}O_2(t)}{K_cO_2 + P_{c1}O_2(t)}\right)$$
$$Flux_{c1}O_2(t) = O_2Flux_{c1}(t) + O_2Flux_{c3}(t)$$
$$P_{c1}O_2(t) = f_{imp}(S_{O_2}, O_2Mb_{maxc1}(t), P_{50c}, C_{c1}O_2(t), V_{c1})$$

[See section "Special Functions" (F.3) for description of f_{imp}]

$$
\begin{aligned}
C^{d}_{c1}O_2(t) &= C_{c1}O_2(t) - O_2Mb_{c1}(t)\\
C^{d}_{c1}CO(t) &= S_{CO}\cdot P_{c1}CO(t)\\
O_2Mb_{maxc1}(t) &= CMb_{maxc} - COMb_{c1}(t)\\
CMb_{maxc} &= \frac{64500}{17000}\left(\frac{K_{O_2}}{4}\cdot C_{Mbc}\right)\\
COMb_{c1}(t) &= C_{c1}CO(t) - (S_{CO}\cdot P_{c1}CO(t))\\
P_{c1}CO(t) &= \left(\frac{P_{c1}O_2(t)}{M_M}\right)\cdot\left(\frac{COMb_{c1}(t)}{O_2Mb_{c1}(t)}\right)\\
O_2Mb_{c1}(t) &= O_2Mb_{maxc1}(t)\cdot\left(\frac{P_{c1}O_2(t)}{P_{50c}+P_{c1}O_2(t)}\right)\\
D'_cO_2 &= 600\cdot DO_2\\
Flux_{c1}CO(t) &= COFlux_{c1}(t) + COFlux_{c3}(t)\\
D'_cCO &= 0.75D'_cO_2\\
C_{c1}O_2(t) &= O_2Mb_{c1}(t) + S_{O_2}\cdot P_{c1}O_2(t)\\
C_{c1}CO(t) &= COMb_{c1}(t) + S_{CO}\cdot P_{c1}CO(t)
\end{aligned}
$$

Auxiliary Equations Cardiac Tissue Compartment 2, c_2

$$
\begin{aligned}
V_{c2} &= (1-Fv_c)\cdot V_c\\
MR_{c2}O_2 &= (MR_cO_2)\cdot\frac{V_{c2}}{V_{c1}+V_{c2}}\\
C^{d}_{c2}O_2(t) &= C_{c2}O_2(t) - O_2Mb_{c2}(t)\\
C^{d}_{c2}CO(t) &= S_{CO}\cdot P_{c2}CO(t)\\
Flux_{c2}O_2(t) &= O_2Flux_{c2}(t)\\
Flux_{c2}CO(t) &= COFlux_{c2}(t)
\end{aligned}
$$

All other equations are similar to those of cardiac tissue compartment 1.

Auxiliary Equations Cardiac Blood Compartment 1, bc_1

$$
\begin{aligned}
O_2Flux_{c1}(t) &= Db_{c1}O_2(t)\cdot(P_{a1c}O_2(t) - P_{c1}O_2(t))\\
P_{a1c}O_2(t) &= f_{\text{getPavg}}(O_2Hb_{maxc1}(t), Vb_{c1}, P_{50}(t), n(t),\\
&\quad C_{c1av}O_2(t), S_{O_2}, P_{ar}O_2(t), P_{cv1}O_2(t))
\end{aligned}
$$

[See section "Special Functions" (F.5) for description of f_{getPavg}]

$$
\begin{aligned}
O_2Hb_{maxc1}(t) &= O_2Hb_{max} - COHb(t)\\
C_{c1av}O_2(t) &= 0.5(C_{ar}O_2(t) + C_{cv1}O_2(t))\\
\dot{Q}_c(t) &= \dot{Q}_{c0}\cdot[1 + 0.572(\%COHb(t))]\\
\dot{Q}_{c0} &= \left(\frac{[2.18(HR) - 27.3]}{100}\right)\cdot V_c\\
V_{bc1} &= F_{vc}\cdot V_{bc}\\
Vb_c &= \text{volfrac}_c\cdot V_c
\end{aligned}
$$

$$
\begin{aligned}
&[P_{cv1}O_2(t), O_2Hb_{cv1}(t)]\\
&\quad = f_{\text{getPO}_2}(O_2Hb_{ar}(t), P_{50}(t), n(t), O_2Hb_{maxc1}(t), S_{O_2},\\
&\quad P_{ar}O_2(t), \dot{Q}_c(t))
\end{aligned}
$$

[See section "Special Functions" (F.4) for description of f_{getPO_2}]

$$
\begin{aligned}
Db_{c1}O_2(t) &= \frac{PS_{c1}O_2(t)\cdot S_{O_2}\cdot V_{c1}}{1.04}\\
PS_{c1}O_2(t) &= PS_{cav\_rest}\cdot\frac{\dot{Q}_c(t)}{\dot{Q}_{c0}}\\
COFlux_{c1}(t) &= Db_{c1}CO(t)\cdot(P_{a1c}CO(t) - P_{c1}CO(t))\\
Db_{c1}CO(t) &= D_cCO(t)\cdot\left(\frac{Db_{c1}O_2(t)}{Db_{c2}O_2(t)}\right)\\
D_cCO(t) &= D_MCO\cdot\left(\frac{Db_{c2}O_2(t)}{Db_{m2}O_2(t)}\right)\\
P_{a1c}CO(t) &= 0.5(P_{ar}CO(t) + P_{cv1}CO(t))\\
P_{cv1}CO(t) &= \left(\frac{P_{cv1}O_2(t)}{M_H}\right)\cdot\left(\frac{COHb_{cv1}(t)}{O_2Hb_{cv1}(t)}\right)\\
COHb_{cv1}(t) &= C_{cv1}CO(t) - (S_{CO}\cdot P_{cv1}CO(t))
\end{aligned}
$$

Auxiliary Equations Cardiac Blood Compartment 2, bc_2

$$
\begin{aligned}
O_2Flux_{c2}(t) &= Db_{c2}O_2\cdot(P_{a2c}O_2(t) - P_{c2}O_2(t))\\
V_{bc2} &= (1-F_{vc})\cdot V_{bc}\\
Db_{c2}O_2(t) &= \frac{PS_{c2}O_2(t)\cdot S_{O_2}\cdot V_{c2}}{1.04}\\
PS_{c2}O_2(t) &= PS_{ccap\_rest}\cdot\frac{\dot{Q}_c(t)}{\dot{Q}_{c0}}\\
COFlux_{c2}(t) &= Db_{c2}CO(t)\cdot(P_{a2c}CO(t) - P_{c2}CO(t))\\
Db_{c2}CO(t) &= D_cCO(t)
\end{aligned}
$$

All other equations are similar to those of cardiac blood compartment 1.

Auxiliary Equations Cardiac Blood Compartment 3, bc_3

$$
\begin{aligned}
O_2Flux_{c3}(t) &= Db_{c3}O_2(t)\cdot(P_{a3c}O_2(t) - P_{c1}O_2(t))\\
V_{bc3} &= D_{bvc\_on}\cdot V_{bc1}\\
Db_{c3}O_2(t) &= D_{bvc\_on}\cdot Db_{c1}O_2(t)\\
COFlux_{c3}(t) &= D_{bc3}CO(t)\cdot(P_{a3c}CO(t) - P_{c1}CO(t))\\
Db_{c3}CO(t) &= D_cCO(t)\cdot\left(\frac{Db_{c3}O_2(t)}{Db_{c2}O_2(t)}\right)
\end{aligned}
$$

All other equations are similar to those of cardiac blood compartment 1.

Other Tissue Compartment, (ot)

$$V_{\mathrm{ot}}\frac{dC_{\mathrm{ot}}\mathrm{O_2}(t)}{dt} = \mathrm{O_2flux_{ot}}(t) - MR_{\mathrm{ot}}\mathrm{O_2} \tag{B.25}$$

$$V_{\mathrm{ot}}\frac{dC_{\mathrm{ot}}\mathrm{CO}(t)}{dt} = \mathrm{COflux_{ot}}(t) \tag{B.26}$$

Auxiliary Equations for Other Tissue (Nonmuscle) Compartment

$$MR_{\mathrm{ot}}\mathrm{O_2} = MR\mathrm{O_2} - (MR_{\mathrm{m}}\mathrm{O_2} + MR_{\mathrm{c}}\mathrm{O_2})$$
$$\mathrm{O_2flux_{ot}}(t) = \left[\mathrm{P_{ot\_avg}O_2}(t) - \mathrm{P_{ot}O_2}(t)\right] \cdot D\mathrm{b_{ot}O_2}$$
$$\mathrm{P_{ot\_avg}O_2}(t) = f_{\mathrm{pinv}}\left(\mathrm{O_2Hb_{ot}}(t), \mathrm{P_{50}}(t), n(t), C_{\mathrm{maxot}}(t)\right)$$

[See section "Special Functions" (F.2) for description of f_{pinv}]

$$\mathrm{O_2Hb_{ot}}(t) = 0.5(\mathrm{O_2Hb_{ar}}(t) + \mathrm{O_2Hb_{vot}}(t))$$
$$\tau_{\mathrm{ot}}\frac{d\mathrm{O_2Hb_{vot}}(t)}{dt} + \mathrm{O_2Hb_{vot}}(t) = \mathrm{O_2Hb_{votun}}(t)$$
$$[\mathrm{P_{vot}O_2}(t), \mathrm{O_2Hb_{votun}}(t)] = f_{\mathrm{getPO_2}}(\mathrm{O_2Hb_{ar}}(t), \mathrm{P_{50}}(t), n(t), C_{\mathrm{maxot}}(t), \mathrm{S_{O_2}}, \mathrm{P_{ar}O_2}(t), \dot{Q}_{\mathrm{ot}}(t))$$

[See section "Special Functions" (F.4) for description of $f_{\mathrm{getPO_2}}$]

$$C_{\mathrm{maxot}}(t) = \mathrm{O_2Hb_{max}} - \mathrm{COHb_{vot}}(t)$$
$$\tau_{\mathrm{ot}}\frac{d\mathrm{COHb_{vot}}(t)}{dt} + \mathrm{COHb_{vot}}(t) = \mathrm{COHb_{votun}}(t)$$
$$\mathrm{COHb_{votun}}(t) = C_{\mathrm{ar}}\mathrm{CO}(t) - \mathrm{S_{CO}} \cdot \mathrm{P_{vot}CO}(t) - \frac{\mathrm{COflux_{ot}}(t)}{\dot{Q}_{\mathrm{ot}}(t)}$$
$$\dot{Q}_{\mathrm{ot}}(t) = \dot{Q}(t) - \left(\dot{Q}_{\mathrm{m}}(t) + \dot{Q}_{\mathrm{c}}(t)\right)$$
$$\mathrm{P_{vot}CO}(t) = \left(\frac{\mathrm{P_{vot}O_2}(t)}{M_{\mathrm{H}}}\right) \cdot \left(\frac{\mathrm{COHb_{vot}}(t)}{\mathrm{O_2Hb_{vot}}(t)}\right)$$
$$\mathrm{COflux_{ot}}(t) = D\mathrm{b_{ot}CO} \cdot (\mathrm{P_{bot}CO}(t) - \mathrm{P_{ot}CO}(t))$$
$$D\mathrm{b_{ot}CO} = D_{\mathrm{M}}\mathrm{CO} \cdot \left(\frac{V_{\mathrm{ot}}}{V_{\mathrm{m}}}\right)$$
$$V_{\mathrm{ot}} = V_{\mathrm{m}} \cdot \left(\frac{V_{\mathrm{ot_0}}}{V_{\mathrm{m_0}}}\right)$$
$$\mathrm{P_{bot}CO}(t) = 0.5(\mathrm{P_{ar}CO}(t) + \mathrm{P_{vot}CO}(t))$$
$$\mathrm{P_{ot}O_2}(t) = \frac{C_{\mathrm{ot}}\mathrm{O_2}(t)}{\mathrm{S_{O_2}}}$$
$$C_{\mathrm{vot}}\mathrm{O_2}(t) = \mathrm{P_{vot}O_2}(t) \cdot \mathrm{S_{O_2}}$$
$$\mathrm{P_{ot}CO}(t) = \frac{C_{\mathrm{ot}}\mathrm{CO}(t)}{\mathrm{S_{CO}}}$$
$$C_{\mathrm{vot}}\mathrm{CO}(t) = \mathrm{P_{vot}CO}(t) \cdot \mathrm{S_{CO}}$$
$$\tau_{\mathrm{ot}} = \frac{V_{\mathrm{bot}}}{\dot{Q}_{\mathrm{ot}}(t)}$$
$$V_{\mathrm{bot}} = \mathrm{Volfrac_{ot}} \cdot V_{\mathrm{ot}}$$

Mixed Venous Blood compartment, (mx)

$$V_{\mathrm{mx}}\frac{dC_{\mathrm{mx}}\mathrm{O_2}(t)}{dt} = \dot{Q}(t) \cdot (C_{\mathrm{mx\_in}}\mathrm{O_2}(t) - C_{\mathrm{mx}}\mathrm{O_2}(t)) \tag{B.27}$$

$$V_{\mathrm{mx}}\frac{dC_{\mathrm{mx}}\mathrm{CO}(t)}{dt} = \dot{Q}(t) \cdot (C_{\mathrm{mx\_in}}\mathrm{CO}(t) - C_{\mathrm{mx}}\mathrm{CO}(t)) \tag{B.28}$$

Auxiliary Equations for Mixed Venous Compartment

$$C_{\mathrm{mx\_in}}\mathrm{O_2}(t) = C_{\mathrm{vot}}\mathrm{O_2}(t) \cdot \left(\frac{\dot{Q}_{\mathrm{ot}}(t)}{\dot{Q}(t)}\right) + C_{\mathrm{mv3}}\mathrm{O_2}(t) \cdot \left(\frac{\dot{Q}_{\mathrm{m}}(t)}{\dot{Q}(t)}\right) + C_{\mathrm{cv3}}\mathrm{O_2}(t) \cdot \left(\frac{\dot{Q}_{\mathrm{c}}(t)}{\dot{Q}(t)}\right)$$
$$\tau_{\mathrm{mx}} = \frac{\mathrm{V_{mx}}}{\dot{Q}(t)}$$
$$V_{\mathrm{mx}} = 0.75 \cdot (V_{\mathrm{b}} - V_{\mathrm{bm}} - V_{\mathrm{bot}})$$
$$\mathrm{P_{mx}O_2}(t) = f_{\mathrm{imp}}(\mathrm{S_{O_2}}, C_{\mathrm{maxmx}}(t), \mathrm{P_{50}}(t), n(t), C_{\mathrm{mx}}\mathrm{O_2}(t), V_{\mathrm{mx}})$$

[See section "Special Functions" (F.3) for description of f_{imp}]

$$C_{\mathrm{maxmx}}(t) = \mathrm{O_2Hb_{max}} - \mathrm{COHb_{mx}}(t)$$
$$\mathrm{COHb_{mx}}(t) = \mathrm{COHb_{vot}}(t) \cdot \left(\frac{\dot{Q}_{\mathrm{ot}}(t)}{\dot{Q}(t)}\right) + \mathrm{COHb_{mv3}}(t) \cdot \left(\frac{\dot{Q}_{\mathrm{m}}(t)}{\dot{Q}(t)}\right) + \mathrm{COHb_{cv3}}(t) \cdot \left(\frac{\dot{Q}_{\mathrm{c}}(t)}{\dot{Q}(t)}\right) + \left(\frac{\dot{V}\mathrm{co}}{\dot{Q}(t)}\right)$$

$$P_{mx}CO(t) = \left(\frac{P_{mx}O_2(t)}{M_H}\right) \cdot \left(\frac{COHb_{mx}(t)}{O_2Hb_{mx}(t)}\right)$$

$$O_2Hb_{mx}(t) = f_{odc}(P_{mx}O_2(t), P_{50}(t), n(t), C_{maxmx}(t))$$

[See section "Special Functions" (F.1) for description of f_{odc}]

$$C_{mx\_in}CO(t) = C_{vot}CO(t) \cdot \left(\frac{\dot{Q}_{ot}(t)}{\dot{Q}(t)}\right) + C_{mv3}CO(t) \cdot \left(\frac{\dot{Q}_m(t)}{\dot{Q}(t)}\right) + C_{cv3}CO(t) \cdot \left(\frac{\dot{Q}_c(t)}{\dot{Q}(t)}\right)$$

Special Functions

$$f_{odc} : O_2Hb = f_{odc}(PO_2, P_{50}, n, C_{max}) \quad \text{(F.1)}$$

f_{odc} calculates concentration of O_2 bound to hemoglobin, O_2Hb (oxyhemoglobin), from the oxygen dissociation curve (ODC) of Hb as $O_2Hb = C_{max} \cdot \left(\frac{\left(\frac{PO_2}{P_{50}}\right)^n}{1+\left(\frac{PO_2}{P_{50}}\right)^n}\right)\left(1 + \left(0.25 + \left(\frac{5PO_2}{P_{50}}\right)^3\right)^{-1}\right)$ where the values specified for C_{max} (Maximum concentration of Hb bound to O_2 excluding the Hb bound to CO), P_{50} (Partial pressure of oxygen at 50% of Hb saturation), and n (Hill exponent for Hb) represent the vascular compartment of interest and are all functions of %COHb(t) (See Appendix B, section "Lung (Alveolar (L) and End-Pulmonary (ep)) Compartments"). The second term in brackets applies only when $n > 1.1$.

$$f_{pinv} : PO_2 = f_{pinv}(O_2Hb, P_{50}, n, C_{max}) \quad \text{(F.2)}$$

f_{pinv} calculates blood PO_2 (Partial pressure of oxygen) corresponding to a given oxyhemoglobin content as $P^*O_2 = P_{50} \cdot \left(\frac{O_2Hb}{C_{max} - O_2Hb}\right)^{\frac{1}{n}}$ where the values specified for C_{max}, P_{50}, and n represent the vascular compartment of interest and are all functions of %COHb(t) (See Appendix B, section "Lung (Alveolar (L) and End-Pulmonary (ep)) Compartments"). If $P^*O_2 <$ 20 Torr, then $PO_2 = \frac{P^*O_{2(t)}}{1 + \left(0.25 + \left(\frac{5P^*O_2}{P_{50}}\right)^3\right)^{-1}}$.

Otherwise, $PO_2 = P^*O_2$.

$$f_{imp} : PO_{2(P_{bi}O_2 \text{ or } P_{ti}O_2)} = f_{imp}\left(S_{O_2}, C_{max(C_{maxbi} \text{ or } O_2Mb_{maxi})}, P_{50}, n, C_{O_2(C_{bi}O_2 \text{ or } C_{ti}O_2)}\right) \quad \text{(F.3)}$$

f_{imp} is an ACSL operator which finds an implicit solution to a nonlinear algebraic equation involving a single unknown variable (in our case, blood ($P_{bi}O_2(t)$) or tissue ($P_{t_i}O_2(t)$) partial pressure of oxygen). The algebraic expression solved implements the concept that the total concentration of O_2 (C_{O_2}) in a given compartment (blood or tissue) equals to the concentration of O_2 dissolved and the concentration of O_2 bound to heme protein (Hb or Mb) in that compartment. These expressions are:

For blood compartment "bi" at time "t":

$$(P_{bi}O_2(t) \cdot S_{O_2}) + \left(C_{max\,bi}(t) \cdot \left[\frac{\left(\frac{P_{bi}O_2(t)}{P_{50}(t)}\right)^{n(t)}}{1 + \left(\frac{P_{bi}O_2(t)}{P_{50}(t)}\right)^{n(t)}}\right]\right) - C_{bi}O_2(t) = 0$$

where $P_{bi}O_2(t), C_{bi}O_2(t)$ are the PO_2 and O_2 concentration in the blood compartment 'i'

For tissue compartment "ti" at time "t":

$$(P_{ti}O_2(t) \cdot S_{O_2} \cdot V_{ti}) + \left(O_2Mb_{max\,i}(t) \cdot V_{ti} \cdot \left[\frac{P_{ti}O_2(t)}{P_{50m} + P_{ti}O_2(t)}\right]\right) - (C_{ti}O_2(t) \cdot V_{ti}) = 0$$

where, $P_{ti}O_2(t), C_{ti}O_2(t)$ are the PO_2 and O_2 concentration in the tissue compartment 'i'.

$$f_{getPO_2} : [PO_2, O_2Hb] = f_{getPO_2}(O_2Hb_{b(in)}, P_{50}, n, O_2Hb_{max}, S_{O_2}, P_{b(in)}O_2, \dot{Q}_i) \quad \text{(F.4)}$$

f_{getPO_2} calculates $P_{bi}O_2$(t) and O_2Hb_{bi}(t) in the venous outflow from blood subcompartments of muscle compartment, with inflowing blood described by $P_{b(in)}O_2$ and O_2Hb_{in}, while accounting for tissue exchange of oxygen with blood, oxygen combined with Hb, and oxygen dissolved in plasma. Two (total O_2 content, Haldane equation) simultaneous algebraic equations of PO_2 are solved iteratively under the constraint that change in total oxygen content of the blood, multiplied by blood flow, must equal the blood-to-tissue oxygen flux (predetermined on the basis of mean partial pressure gradients). $\dot{Q}_i$ is the blood flow to the compartment i.

Total O_2 content:

$$C_{O_2} = \frac{C_{O_{2(max)}} \cdot \left(\frac{PO_2}{P_{50}}\right)^n}{1 + \left(\frac{PO_2}{P_{50}}\right)^n} + S_{O_2} \cdot PO_2;$$

Haldane equation: $\frac{M_H \cdot PCO}{COHb} = \frac{PO_2}{O_2Hb}$

A gradient search method is used. The iterations terminate when a solution for PO_2 is reached within the limits of a specified tolerance (0.01 Torr). An error flag is set if the maximum iteration number (10,000) is reached. O_2Hb is calculated from the determined PO_2 using the f_{odc} function.

$$f_{getPavg} : P_{avgi} = f_{getPavg}(O_2Hb_{max\,i}, Vb_i, P_{50}, n, C_{iav}O_2, S_{O_2}, P_{b(i-1)}O_2, P_{bi}O_2) \quad (F.5)$$

$f_{getPavg}$ calculates average vascular PO_2, $P_{avgi}(t)$, in the blood subcompartments of the tissue. $P_{avgi}(t)$ is the partial pressure of O_2 corresponding to the concentration of O_2, $C_{iav}O_2(t)$, halfway between the inlet (subscript "i − 1") and outlet (subscript "i") concentrations of the vascular subcompartment 'i'. $P_{avgi}(t)$ takes into account O_2 dissolved as well as O_2 bound to hemoglobin. A dichotomous search method is used to determine $P_{avgi}(t)$. Vb_i is the volume of blood in compartment i.

APPENDIX C: PARAMETER ESTIMATES BASED ON REGRESSION EQUATIONS[1]

This section contains the regression equations used in the model to estimate certain parameter values, when those values are not reported in the experimental studies.

Volume of muscle tissue, V_m (mL):

$$V_m = [1000(0.244\,BW + 7.80\,HT + 6.6G - 0.098\,A - 3.3)]/1.04 \quad (C.1)$$

$$V_{m\_obese} = (V_m - 8706.9)/0.805$$

BW = Body Weight in kg; HT = Height in cm; G = 0: Female; 1: Male; A = Age in years

Volume of leg muscle tissue, V_{lm} (ml):

$$\text{For Male, } V_{lm} = 0.4663(V_m); \quad \text{For Female, } V_{lm} = 0.4953(V_m) \quad (C.1.1)$$

Volume of arm muscle tissue, V_{am} (ml):

$$\text{For Male, } V_{am} = (0.1564 * V_m); \quad \text{For Female, } V_{am} = (0.1396 * V_m) \quad (C.1.2)$$

Volume of trunk muscle tissue, V_{tm} (ml):

$$\text{For Male, } V_{tm} = (0.3773 * V_m); \quad \text{For Female, } V_{tm} = (0.3651 * V_m) \quad (C.1.3)$$

Total body volume of blood, V_b (mL):

$$V_b = 70\left(\sqrt{\frac{BMI\_p}{22(HT)^2}}\right)^{-1} \quad (C.2)$$

$$BMI\_p = \left(\frac{delta\_IBW}{100}\right)22 + 22$$

$$delta\_IBW = \left(\frac{BMI}{22}\right)100$$

$$BMI = \frac{BW}{(HT)^2}$$

Cardiac Output, $\dot{Q}_0$ (L/min):

$$\dot{Q}_0 = (54.1 + 7.9G) \cdot BW + 1400 - 200 \cdot G \quad (C.3)$$

During exercise;

$$\dot{Q}_0 = 3.186 + 7.346(MRO_2) - 0.535(MRO_2)^2 \quad (C.4)$$

MRO_2 = Total Body Metabolic Rate in STPD, L/min

The changes in cardiac output $(\dot{Q})$ with CO exposure were implemented in our previous model.[8] Our objective in this study was to simulate changes in $\dot{Q}$ in response to physical activity. In order to account for change in cardiac output with physical activity, we developed a predictive equation for estimating cardiac output, $\dot{Q}$, as a function of total body oxygen consumption, MRO_2. Rest and exercise data for cardiac output and MRO_2 from various published papers[3,4,6,18,21,34,37,72] from human subjects are shown in Fig. 14. The developed prediction equation, based on a nonlinear, least squares polynomial fit, is Eq. (C.4). Cardiac output was measured either by dye dilution, transthoracic electric bioimpedance, or Fick's method. The data were obtained from healthy, non-smoking, untrained individual subjects. As shown in Fig. 14, cardiac output reaches a plateau as maximal body O_2 consumption is reached. Eq. (C.3) was used in simulation of Burge and Skinner[11] and Eq. (C.4) was not used in any of the simulations of the manuscript.

Percent change in Cardiac Output with CO exposure:

$$\%\Delta\dot{Q} = 0.572\,(\%COHb) \quad (C.5)$$

Heart Rate, HR (beats/min):

$$HR = 42.819 + 68.884(MRO_2) - 8.26(MRO_2)^2 \quad (C.6)$$

[1]Eqs. (C.3) to (C.4) and Eq. (C.6) are used to estimate parameter values only when their values are not provided by the experimental study being simulated.

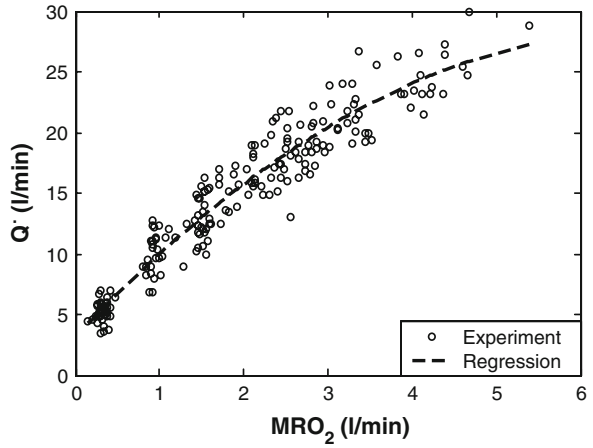

FIGURE 14. Cardiac output ($\dot{Q}$) vs. body oxygen consumption (MRO_2). The data (○) used to build the relationship[3,4,6,18,21,34,37,72] and the regression line. The regression equation is given by $\dot{Q} = 3.186 + 7.346(MRO_2) - 0.535(MRO_2)^2$. See Appendix C for details.

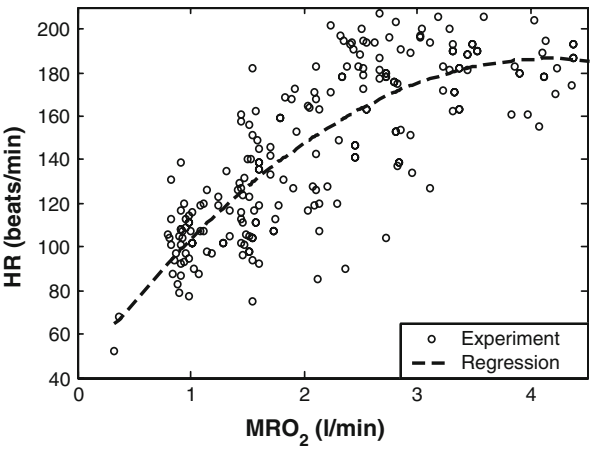

FIGURE 15. Heart rate (HR) vs. body oxygen consumption (MRO_2). The data (○) used to build the relationship.[14,50,83] The regression equation is given by $HR = 42.819 + 68.884(MRO_2) - 8.26(MRO_2)^2$. See Appendix C for details.

In our enhanced model, MBF and MOC for the cardiac compartment were estimated from heart rate. In order to develop a predictive equation for estimating HR, we collected data from the literature[14,50,83] for HR and total body metabolic rate of human subjects during rest and exercise. The polynomial fit to experimental data (Fig. 15) is Eq. (C.6). In most of our simulations, HR was provided to us by the investigators. However, in experiments where heart rate was not measured, it was estimated from the prediction equation. An heart rate of 66 beats/min was assumed for simulations[7,11] when MRO_2 was not measured.

Myocardial Blood Flow, MBF ($mL\ min^{-1}\ g^{-1}$):

$$\mathrm{MBF} = 2.18(HR) - 27.3 \qquad \text{(C.7)}$$

Myocardial Oxygen Consumption, MOC ($mL\ min^{-1}\ g^{-1}$):

$$\mathrm{MOC} = \frac{46.6}{1 + \left(\frac{122.7}{HR}\right)^{4.85}} + 9.76 \qquad \text{(C.8)}$$

ACKNOWLEDGMENTS

This research was supported in part by a Grant from NIOSH (OH 008651). The authors thank Dr. Vernon Benignus (US EPA, Research Triangle Park), Dr. Caroline Burge (University of Melbourne, Australia), Dr. Paul Kizakevich (RTI, Research Triangle Park, NC), and Dr. Marko Laaksonen (Turku PET Center, University of Turku, Finland) for providing both data published in their papers[7,11,50,54] and unpublished measurements of parameter values from their subjects. The code and the command files of the computational model are available for download on http://www.acslx-wiki.com/dokuwiki/doku.php?id=models:pbpk:extravascularco

REFERENCES

[1]Agata, H., T. Ichinohe, and Y. Kaneko. Felypressin-induced reduction in coronary blood flow and myocardial tissue oxygen tension during anesthesia in dogs. *Can. J. Anaesth.* 46(11):1070–1075, 1999.

[2]Anderson, R. F., D. C. Allensworth, and W. J. DeGroot. Myocardial toxicity from carbon monoxide poisoning. *Ann. Intern. Med.* 67(6):1172–1182, 1967.

[3]Astrand, P. O., T. E. Cuddy, B. Saltin, and J. Stenberg. Cardiac output during submaximal and maximal work. *J. Appl. Physiol.* 19:268–274, 1964.

[4]Barker, R. C., S. R. Hopkins, N. Kellogg, I. M. Olfert, T. D. Brutsaert, T. P. Gavin, P. L. Entin, A. J. Rice, and P. D. Wagner. Measurement of cardiac output during exercise by open-circuit acetylene uptake. *J. Appl. Physiol.* 87(4):1506–1512, 1999.

[5]Beard, D. A., and J. B. Bassingthwaighte. Advection and diffusion of substances in biological tissues with complex vascular networks. *Ann. Biomed. Eng.* 28:253–268, 2000.

[6]Beck, K. C., L. N. Randolph, K. R. Bailey, C. M. Wood, E. M. Snyder, and B. D. Johnson. Relationship between cardiac output and oxygen consumption during upright cycle exercise in healthy humans. *J. Appl. Physiol.* 101(5): 1474–1480, 2006.

[7]Benignus, V. A., M. J. Hazucha, M. V. Smith, and P. A. Bromberg. Prediction of carboxyhemoglobin formation due to transient exposure to carbon monoxide. *J. Appl. Physiol.* 76(4):1739–1745, 1994.

[8]Bruce, E. N., M. C. Bruce, and K. Erupaka. Prediction of the rate of uptake of carbon monoxide from blood by extravascular tissues. *Respir. Physiol. Neurobiol.* 161(2): 142–159, 2008.

[9]Bruce, E. N., and M. C. Bruce. A multicompartment model of carboxyhemoglobin and carboxymyoglobin

responses to inhalation of carbon monoxide. *J. Appl. Physiol.* 95(3):1235–1247, 2003.
[10]Bruce, M. C., and E. N. Bruce. Analysis of factors that influence rates of carbon monoxide uptake, distribution, and washout from blood and extravascular tissues using a multicompartment model. *J. Appl. Physiol.* 100(4):1171–1180, 2006.
[11]Burge, C. M., and S. L. Skinner. Determination of hemoglobin mass and blood volume with CO: evaluation and application of a method. *J. Appl. Physiol.* 79(2):623–631, 1995.
[12]Caldwell, J. H., G. V. Martin, G. M. Raymond, and J. B. Bassingthwaighte. Regional myocardial flow and capillary permeability surface area products are nearly proportional. *Am. J. Physiol.* 267:H654–H666, 1994.
[13]Cerretelli, P., and M. Samaja. Acid–base balance at exercise in normoxia and in chronic hypoxia. Revisiting the "lactate paradox". *Eur. J. Appl. Physiol.* 90(5–6):431–448, 2003.
[14]Chiodi, H., D. B. Dill, F. Consolazio, and S. M. Horvath. Respiratory and circulatory responses to acute carbon monoxide poisoning. *Am. J. Physiol.* 134:H683–H693, 1941.
[15]Choi, I. S. Delayed neurologic sequelae in carbon monoxide intoxication. *Arch. Neurol.* 40:433–435, 1983.
[16]Chung, Y., S. J. Huang, A. Glabe, and T. Jue. Implication of CO inactivation on myoglobin function. *Am. J. Physiol. Cell. Physiol.* 290(6):C1616–C1624, 2006.
[17]Cosby, R., and M. Bergeron. Electrocardiographic changes in carbon monoxide. *Am. J. Cardiol.* 11:93–96, 1963.
[18]Crisafulli, A., F. Melis, F. Tocco, U. M. Santoboni, F. Frongia, C. Carta, M. Caddeo, and A. Concu. Anaerobic threshold and the oxygen consumption–cardiac output relationship during exercise. *Sport Sci. Health* 2:75–80, 2005.
[19]Dash, R. K., and J. B. Bassingthwaighte. Blood HbO_2 and $HbCO_2$ dissociation curves at varied O_2, CO_2, pH, 2,3-DPG and temperature levels. *Ann. Biomed. Eng.* 32(12): 1676–1693, 2004.
[20]Edlund, A., and A. Sollevi. Theophylline increases coronary vascular tone in humans: evidence for a role of endogenous adenosine in flow regulation. *Acta. Physiol. Scand.* 155(3):303–311, 1995.
[21]Ekblom, B., P. O. Astrand, B. Saltin, J. Stenberg, and B. Wallstorm. Effect of training on circulatory response to exercise. *J. Appl. Physiol.* 24(4):512–528, 1968.
[22]Endo, M., T. Hino, T. Itaoka, H. Hayashi, and J. Wada. Continuous measurement of human myocardial tissue oxygen tension. *Kokyu To Junkan* 26(9):881–887, 1978.
[23]Faithfull, S., M. Fennema, W. Erdmann, M. Dhasmana, and G. Eilers. The effects of acute ischaemia on intramyocardial oxygen tensions. *Adv. Exp. Med. Biol.* 200:339–348, 1986.
[24]Fitts, R. H. Cellular mechanisms of muscle fatigue. *Physiol. Rev.* 74(1):49–94, 1994.
[25]Gandini, C., A. F. Castoldi, S. M. Candura, S. Priori, C. Locatelli, R. Butera, C. Bellet, and L. Manzo. Cardiac damage in pediatric carbon monoxide poisoning. *J. Toxicol. Clin. Toxicol.* 39(1):45–51, 2001.
[26]Gandini, C., A. F. Castoldi, S. M. Candura, C. Locatelli, R. Butera, S. Priori, and L. Manzo. Carbon monoxide cardiotoxicity. *J. Toxicol. Clin. Toxicol.* 39(1):35–44, 2001.
[27]Gayeski, T. E., and C. R. Honig. Intracellular PO_2 in individual cardiac myocytes in dogs, cats, rabbits, ferrets, and rats. *Am. J. Physiol. Heart. Circ. Physiol.* 260:522–531, 1991.
[28]Giardina, B., P. Ascenzi, M. E. Clementi, G. De Sanctis, M. Rizzi, and M. Coletta. Functional modulation by lactate of myoglobin. A monomeric allosteric hemoprotein. *J. Biol. Chem.* 271(29):16999–17001, 1996.
[29]Gonschior, P., G. M. Gonschior, P. F. Conzen, J. Hobbhahn, A. E. Goetz, K. Peter, and W. Brendel. Myocardial oxygenation and transmural lactate metabolism during experimental acute coronary stenosis in pigs. *Basic Res. Cardiol.* 87(1):27–37, 1992.
[30]Goodale, W. T., and D. B. Hackel. Measurement of coronary blood flow in dogs and man from rate of myocardial nitrous oxide desaturation. *Circ. Res.* 1(6):502–508, 1953.
[31]Grunewald, W. A., and W. Sowa. Distribution of the myocardial tissue PO_2 in the rat and the inhomogenity of the coronary bed. *Pflugers Arch.* 374:57–66, 1978.
[32]Gu, J. W., M. Shparago, W. Tan, and A. P. Bailey. Tissue endostatin correlates inversely with capillary network in rat heart and skeletal muscles. *Angiogenesis* 9(2):93–99, 2006.
[33]Habazettl, H., P. F. Conzen, H. Baier, M. Christ, B. Vollmar, A. Goetz, K. Peter, and W. Brendel. Epicardial oxygen tensions during changes in arterial PO_2 in pigs. *Adv. Exp. Med. Biol.* 277:437–447, 1990.
[34]Harms, C. A., T. J. Wetter, S. R. McClaran, D. F. Pegelow, G. A. Nickele, W. B. Nelson, P. Hanson, and J. A. Dempsey. Effects of respiratory muscle work on cardiac output and its distribution during maximal exercise. *J. Appl. Physiol.* 85:609–618, 1998.
[35]Heineman, F. W., and R. S. Balaban. Phosphorus-31 nuclear magnetic resonance analysis of transient changes of canine myocardial metabolism in vivo. *J. Clin. Invest.* 85(3):843–852, 1990.
[36]Henry, C. R., D. Satran, B. Lindgren, C. Adkinson, C. I. Nicholson, and T. D. Henry. Myocardial injury and long-term mortality following moderate to severe carbon monoxide poisoning. *JAMA* 295:398–402, 2006.
[37]Hermansen, L., B. Ekblom, and B. Saltin. Cardiac output during submaximal and maximal treadmill and bicycle exercise. *J. Appl. Physiol.* 29(1):82–86, 1970.
[38]Hobbhahn, J., P. F. Conzen, A. Goetz, G. Seidl, P. Gonschior, W. Brendel, and K. Peter. Myocardial surface PO_2—an indicator of myocardial tissue oxygenation? *Cardiovasc. Res.* 23(6):529–540, 1989.
[39]Hoffman, W. E., R. F. Albrecht, and Z. S. Jonjev. Myocardial tissue oxygen during coronary artery constriction and hypotension in dogs. *Acta Anaesthesiol. Scand.* 46(6):707–712, 2002.
[40]Horstick, G., A. Heimann, O. Gotze, G. Hafner, O. Berg, P. Boehmer, P. Becker, H. Darius, H. J. Rupprecht, M. Loos, S. Bhakdi, J. Meyer, and O. Kempski. Intracoronary application of C1 esterase inhibitor improves cardiac function and reduces myocardial necrosis in an experimental model of ischemia and reperfusion. *Circulation* 95(3):701–708, 1997.
[41]Jafri, M. S., S. J. Dudycha, and B. O'Rourke. Cardiac energy metabolism: models of cellular respiration. *Annu. Rev. Biomed. Eng.* 3:57–81, 2001.
[42]Joost, C. J. M., J. Petra, J. L. Mike, and T. H. M. Anton. The content and distribution of troponin I, troponin T, myoglobin, and alpha-hydroxybutyric acid dehydrogenase in the human heart. *Am. J. Clin. Pathol.* 115:770–777, 2001.
[43]Jorgensen, C. R., K. Wang, Y. Wang, F. L. Gobel, R. R. Nelson, and H. Taylor. Effect of propranolol on myocardial

oxygen consumption and its hemodynamic correlates during upright exercise. *Circulation* 48(6):1173–1182, 1973.
[44]Jorgensen, C. R., K. Kitamura, F. L. Gobel, H. L. Taylor, and Y. Wang. Long-term precision of the N_2O method for coronary flow during heavy upright exercise. *J. Appl. Physiol.* 30(3):338–344, 1971.
[45]Juel, C. Regulation of pH in human skeletal muscle: adaptations to physical activity. *Acta Physiol. (Oxf)* 193(1):17–24, 2008.
[46]Juel, C., M. K. Holten, and F. Dela. Effects of strength training on muscle lactate release and MCT1 and MCT4 content in healthy and type 2 diabetic humans. *J. Physiol.* 556(Pt 1):297–304, 2004.
[47]Kalay, N., I. Ozdogru, Y. Cetinkaya, N. K. Eryol, A. Dogan, I. Gul, T. Inanc, I. Ikizceli, A. Oguzhan, and A. Abaci. Cardiovascular effects of carbon monoxide poisoning. *Am. J. Cardiol.* 99(3):322–324, 2007.
[48]Kassab, G. S., D. H. Lin, and Y. C. Fung. Morphometry of pig coronary venous system. *Am. J. Physiol.* 267:2100–2113, 1994.
[49]Kitamura, K., C. R. Jorgensen, F. L. Gobel, H. L. Taylor, and Y. Wang. Hemodynamic correlates of myocardial oxygen consumption during upright exercise. *J. Appl. Physiol.* 32(4):516–522, 1972.
[50]Kizakevich, P. N., M. L. McCartney, M. J. Hazucha, and L. H. Sleet. Noninvasive ambulatory assessment of cardiac function and myocardial ischemia in healthy subjects exposed to carbon monoxide during upper and lower body exercise. *Eur. J. Appl. Physiol.* 83:7–16, 2000.
[51]Koike, A., K. Wasserman, Y. Armon, and D. Weiler-Ravell. The work-rate-dependent effect of carbon monoxide on ventilatory control during exercise. *Respir. Physiol.* 85(2):169–183, 1991.
[52]Korzeniewski, B. Oxygen consumption and metabolite concentrations during transitions between different work intensities in heart. *Am. J. Physiol. Heart Circ. Physiol.* 291(3):H1466–H1474, 2006.
[53]Koskela, R. S. Cardiovascular diseases among foundry workers exposed to carbon monoxide. *Scand. J. Work. Environ. Health.* 20:286–293, 1994.
[54]Laaksonen, M. S., K. K. Kalliokoski, M. Luotolahti, J. Kemppainen, M. Teras, H. Kyrolainen, P. Nuutila, and J. Knuuti. Myocardial perfusion during exercise in endurance-trained and untrained humans. *Regul. Integr. Comp. Physiol.* 293(2):837–843, 2007.
[55]Leem, C. H., D. Lagadic-Gossmann, and R. D. Vaughan-Jones. Characterization of intracellular pH regulation in the guinea-pig ventricular myocyte. *J. Physiol.* 517(Pt 1): 159–180, 1999.
[56]Lemmens, H. J., D. P. Bernstein, and J. B. Brodsky. Estimating blood volume in obese and morbidly obese patients. *Obes. Surg.* 16(6):773–776, 2006.
[57]Li, Z., T. Yipintsoi, and J. B. Bassingthwaighte. Nonlinear model for capillary-tissue oxygen transport and metabolism. *Ann. Biomed. Eng.* 25(4):604–619, 1997.
[58]Losse, B., S. Schuchhardt, and N. Niederle. The oxygen pressure histogram in the left ventricular myocardium of the dog. *Pflugers Arch.* 356(2):121–132, 1975.
[59]Lovering, A. T., M. K. Stickland, and M. W. Eldridge. Intrapulmonary shunt during normoxic and hypoxic exercise in healthy humans. *Adv. Exp. Med. Biol.* 588:31–45, 2006.
[60]Matschke, K., U. Gerk, C. Mrowietz, J. W. Park, and F. Jung. Influence of radiographic contrast media on myocardial oxygen tension: a randomized, NaCl-controlled comparative study of iodixanol versus iomeprol in pigs. *Acta Radiol.* 48(3):292–299, 2007.
[61]McGuire, B. J., and T. W. Secomb. A theoretical model for oxygen transport in skeletal muscle under conditions of high oxygen demand. *J. Appl. Physiol.* 91:2255–2265, 2001.
[62]Middleton, G., D. Ashby, and F. Clark. Delayed and long-lasting electrocardiographic changes in carbonmonoxide poisoning. *Lancet* 1:12–14, 1961.
[63]Minami, H., B. M. Wolska, M. O. Stojanovic, and R. J. Solaro. Reversal of effects of acidosis on contraction of rat heart myocytes by CGP-48506. *Front. Biosci.* 13:5638–5645, 2008.
[64]Moxham, J., and R. F. Armstrong. Continuous monitoring of right atrial oxygen tension in patients with myocardial infarction. *Intensive Care Med.* 7(4):157–164, 1981.
[65]Nelson, R. R., F. L. Gobel, C. R. Jorgensen, K. Wang, Y. Wang, and H. L. Taylor. Hemodynamic predictors of myocardial oxygen consumption during static and dynamic exercise. *Circulation* 50(6):1179–1189, 1974.
[66]Penney, D. G. A review: hemodynamic response to carbon monoxide. *Environ. Health Perspect.* 77:121–130, 1988.
[67]Regan, T., G. Timmis, M. Gray, K. Binak, and H. K. Hellems. Myocardial oxygen consumption during exercise in fasting and lipemic subjects. *J. Clin. Invest.* 40:624–630, 1961.
[68]Reiner, L., A. Mazzoleni, F. L. Rodriguez, and R. R. Freudenthal. The weight of the human heart. I. Normal cases AMA. *Arch. Pathol.* 68(1):58–73, 1959.
[69]Richardson, R. S., E. A. Noyszewski, B. Saltin, and A. J. Gonzalez. Effect of mild carboxy-hemoglobin on exercising skeletal muscle: intravascular and intracellular evidence. *Am. J. Physiol. Regul. Integr. Comp. Physiol.* 283(5):1131–1139, 2002.
[70]Richardson, R. S., S. Duteil, C. Wary, D. W. Wray, J. Hoff, and P. G. Carlier. Human skeletal muscle intracellular oxygenation: the impact of ambient oxygen availability. *J. Physiol.* 571(Pt 2):415–424, 2006.
[71]Richmond, K. N., S. Burnite, and R. M. Lynch. Oxygen sensitivity of mitochondrial metabolic state in isolated skeletal and cardiac myocytes. *Am. J. Physiol.* 273:H1613–H1622, 1997.
[72]Roca, J., A. G. Agusti, A. Alonso, D. C. Poole, C. Viegas, J. A. Barbera, R. Rodriguez-Roisin, A. Ferrer, and P. D. Wagner. Effects of training on muscle O2 transport at VO_2max. *J. Appl. Physiol.* 73(3):1067–1076, 1992.
[73]Sapirstein, L. A., and E. Ogden. Theoretic limitations of the nitrous oxide method for the determination of regional blood flow. *Circ. Res.* 4(3):245–249, 1956.
[74]Satran, D., C. R. Henry, C. Adkinson, C. I. Nicholson, Y. Bracha, and T. D. Henry. Cardiovascular manifestations of moderate to severe carbon monoxide poisoning. *J. Am. Coll. Cardiol.* 45:1513–1516, 2005.
[75]Schenkman, K. A., D. R. Marble, D. H. Burns, and E. O. Feigl. Myoglobin oxygen dissociation by multiwavelength spectroscopy. *J. Appl. Physiol.* 82(1):86–92, 1997.
[76]Stanley, W. C. Myocardial lactate metabolism during exercise. *Med. Sci. Sports Exerc.* 23(8):920–924, 1991.
[77]Stern, F. B., R. A. Lemen, and R. A. Curtis. Exposure of motor vehicle examiners to carbon monoxide: a historical prospective mortality study. *Arch. Environ. Health* 36:59–65, 1981.
[78]Stewart, R. D., J. E. Peterson, T. N. Fisher, M. J. Hosko, E. D. Baretta, H. C. Dodd, and A. A. Herrmann. Experimental human exposure to high concentrations of carbon monoxide. *Arch. Environ. Health.* 26(1):1–7, 1973.

[79]Stickland, M. K., A. T. Lovering, and M. W. Eldridge. Exercise-induced arteriovenous intrapulmonary shunting in dogs. *Am. J. Respir. Crit. Care Med.* 176(3):300–305, 2007.
[80]Takahashi, E., and K. Doi. Impact of diffusional oxygen transport on oxidative metabolism in the heart. *Jpn. J. Physiol.* 48(4):243–252, 1998.
[81]Tokunaga, C., R. M. Bateman, J. Boyd, Y. Wang, J. A. Russell, and K. R. Walley. Albumin resuscitation improves ventricular contractility and myocardial tissue oxygenation in rat endotoxemia. *Crit. Care Med.* 35(5):1341–1347, 2007.
[82]Turek, Z., K. Rakusan, J. Olders, L. Hoofd, and F. Kreuzer. Computed myocardial PO_2 histograms: effects of various geometrical and functional conditions. *J. Appl. Physiol.* 70:1845–1853, 1991.
[83]Vogel, J. A., and M. A. Gleser. Effect of carbon monoxide on oxygen transport during exercise. *J. Appl. Physiol.* 32(2):234–239, 1972.
[84]Walley, K. R., R. M. Collins, D. J. Cooper, and C. B. Warriner. Myocardial anaerobic metabolism occurs at a critical coronary venous PO_2 in pigs. *Am. J. Respir. Crit. Care Med.* 155(1):222–228, 1997.
[85]Weaver, L. K. Carbon monoxide poisoning. *Crit. Care Clin.* 15:297–317, 1999.
[86]Wittenberg, B. A., and J. B. Wittenberg. Oxygen pressure gradients in isolated cardiac myocytes. *J. Biol. Chem.* 260(11):6548–6554, 1985.
[87]Yanir, Y., A. Shupak, A. Abramovich, S. A. Reisner, and A. Lorber. Cardiogenic shock complicating acute carbon monoxide poisoning despite neurologic and metabolic recovery. *Ann. Emerg. Med.* 40:420–424, 2002.
[88]Zavorsky, G. S., K. B. Quiron, P. S. Massarelli, and L. C. Lands. The relationship between single-breath diffusion capacity of the lung for nitric oxide and carbon monoxide during various exercise intensities. *Chest* 125(3):1019–1027, 2004.
[89]Zhang, J., K. Ugurbil, A. H. From, and R. J. Bache. Myocardial oxygenation and high-energy phosphate levels during graded coronary hypoperfusion. *Am. J. Physiol. Heart Circ. Physiol.* 280(1):H318–H326, 2001.
[90]Zhou, L., J. E. Salem, G. M. Saidel, W. C. Stanley, and M. E. Cabrera. Mechanistic model of cardiac energy metabolism predicts localization of glycolysis to cytosolic subdomain during ischemia. *Am. J. Physiol. Heart Circ. Physiol.* 288(5):H2400–H2411, 2005.
[91]Zhou, L., M. E. Cabrera, I. C. Okere, N. Sharma, and W. C. Stanley. Regulation of myocardial substrate metabolism during increased energy expenditure: insights from computational studies. *Am. J. Physiol. Heart Circ. Physiol.* 291(3):H1036–H1046, 2006.
[92]Zhu, N., and H. R. Weiss. Effect of hypoxic and carbon monoxide-induced hypoxia on regional myocardial segment work and O_2 consumption. *Res. Exp. Med.* 194(2):97–107, 1994.